Arterial Spin Labelling Based Cerebral Blood Flow in Depressed Patients Receiving Electroconvulsive Therapy

Eva Aalbregt

A thesis submitted for the degree of *Master of Science*

University of Twente
November 2021

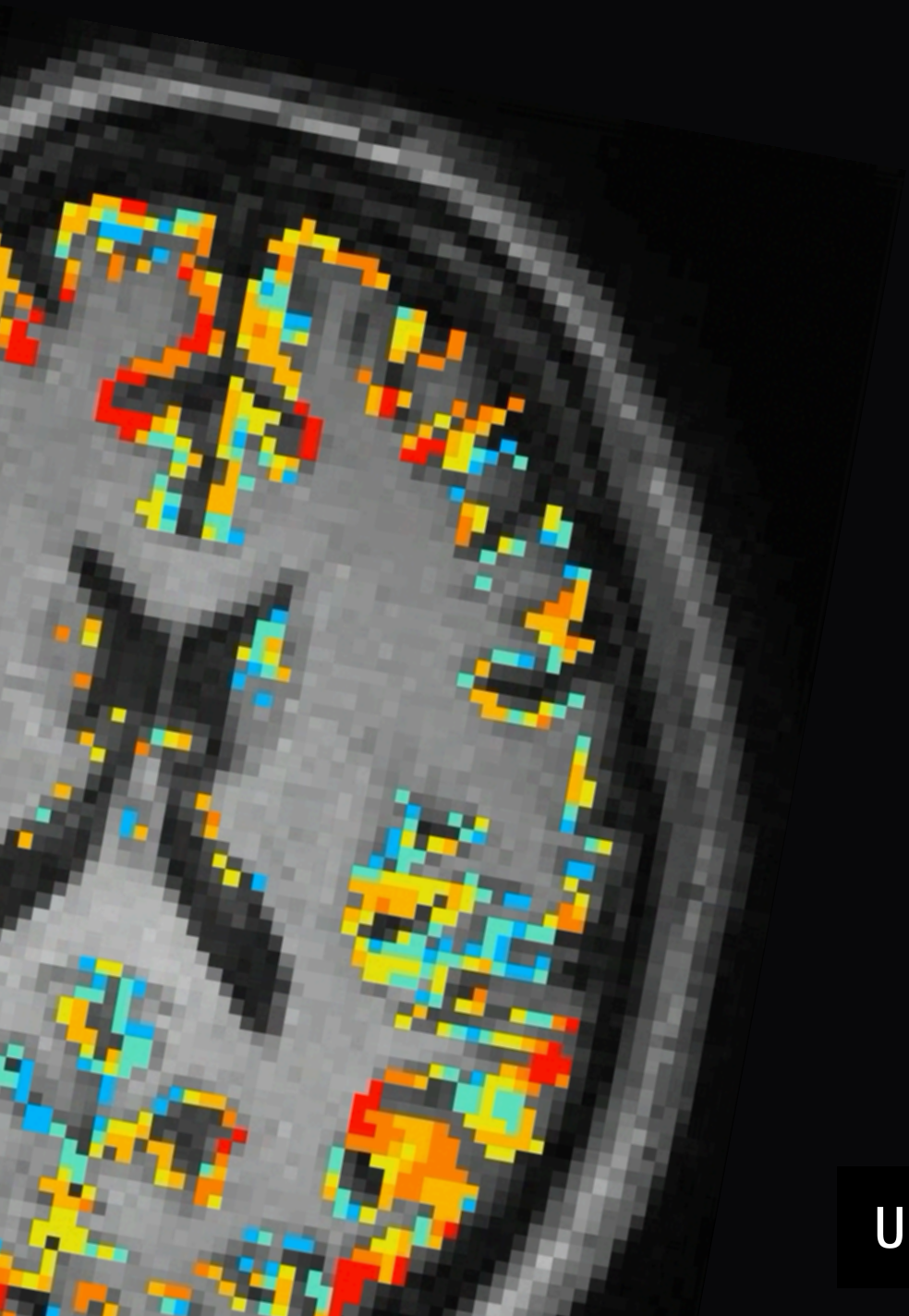

Chairman & Technical Supervisor
prof. dr. ir. M.J.A.M. van Putten

Medical supervisor
prof. dr. J. Hofmeijer

Extra technological supervisor
J.C.M. Pottkämper, MSc.

Process supervisor
drs. P.A. van Katwijk

External member
prof. dr. D.G. Norris

Rijnstate

UNIVERSITEIT TWENTE.

Abstract

Background: Major depressive disorder (MDD) is one of the most prevalent and disabling disorders worldwide. Electroconvulsive therapy (ECT) is an effective treatment option for (therapy-resistant) MDD patients. Often, patients experience postictal symptoms after ECT induced seizures such as cognitive deficits, delirium and headaches. For both, patients and their relatives, the burden of ECT increases with the severity of the postictal symptoms. The mechanisms underlying these symptoms are not yet fully understood. Vasoconstriction-induced hypoperfusion seems to be a candidate mechanism. We were specifically interested in postictal perfusion, based on this hypothesis. Moreover, altered perfusion, also called cerebral blood flow (CBF) has been observed in MDD patients and seems to be related to treatment response. We aim to assess both, the short term (postictal) and long term effects (week to months after treatment) of ECT on the CBF.
Methods: To assess perfusion, patients typically underwent six arterial spin labelling magnetic resonance imaging (ASL MRI) scans. Baseline scans were acquired before the start of the first ECT session. Three MRI scans were made one hour after an ECT induced seizure (postictal), one within two weeks after ECT termination (end-ECT), and the last three months thereafter (follow-up). An automated imaging pipeline was created to calculate global and regional CBF (gCBF and rCBF, respectively). Linear mixed-effects models were utilised for the statistical analyses. Several factors such as seizure duration and electrode placement were included as fixed effects to find possible correlations with postictal gCBF. For the long term effects the antidepressant effect of ECT was assessed with the Hamilton Rating Scale for Depression (HRSD). A decrease in HRSD-score of 50% at end-ECT compared to baseline was considered treatment response. Six regions known to have altered rCBF in MDD patients compared to healthy controls were included for regional analyses of long term effects.
Results: In all eleven patients, postictal gCBF was not statistically different from baseline in the included patient population. Longer seizure duration resulted in a lower postictal perfusion ($p = 0.04$). Half of the patients responded to ECT. Normalised gCBF had a statistically significant effect on normalised HRSD-score ($p = 0.02$) in the same time frame. Responders had a lower mean baseline gCBF value compared to non-responders and showed an increase in gCBF over the ECT course. Non-responders showed a decrease in gCBF over the ECT course. Although, the same trends were observed in most included regions these were not statistically significant.
Conclusions: The hypothesised postictal hypoperfusion was not observed in the current study population. Longer seizure duration was correlated with lower postictal gCBF values. The antidepressant effect of ECT seems to be related to overall perfusion, however, this effect could not be replicated regionally.

Contents

List of abbreviations

ASL	arterial spin labelling
ATT	arterial transit time
BET	brain extraction tool
BL	bifrontotemporal
BOLD	Blood Oxygen Level Dependent
CBF	cerebral blood flow
COX-2	cyclooxygenase -2
DSM-5	Diagnostic and Statistical Manual of Mental Disorders fifth edition
EEG	electroencephalogram
ECT	electroconvulsive therapy
gCBF	global cerebral blood flow
GM	grey matter
GRASE	gradient-and-spin-echo
HRSD	Hamilton Rating Scale for Depression
LUL	left unilateral
MDD	Major depressive disorder
MRI	magnetic resonance imaging
pCASL	pseudo-continuous arterial spin labelling
PET	positron emission tomography
PLD	post labelling delay
rCBF	regional cerebral blood flow
RF	radiofrequency
ROI	region of interest
RUL	right unilateral
SE	standard error
SNR	signal to noise ration
SPECT	single-photon emission computed tomography
SYNAPSE	study of effect of Nimodipine and Acetaminophen on Postictal Symptoms after ECT
tBSI	temporal brain symmetry index
TE	echo time
TR	repetition time
WM	white matter
3D	three-dimensional

General introduction

Major depressive disorder

Major depressive disorder (MDD) has a lifetime prevalence between 8-12% in the general population [1]. It is the one of the most prevalent and disabling disorders worldwide, and therefore has a considerable impact on society [2]. A major depressive episode is defined by the Diagnostic and Statistical Manual of Mental Disorders (DSM-5) as a period of at least two weeks wherein a patient experiences (1) a depressed mood or (2) loss of pleasure or interest in activities in addition to at least four more symptoms. Those symptoms include feelings of worthlessness or disproportionate guilt, diminished ability to think, concentrate or decide, significant weight loss or gain or change in appetite, psychomotor agitation or retardation, fatigue or loss of energy and suicidal ideation or specific plans or attempts to commit suicide [3]. Both pharmacotherapy and psychological interventions such as cognitive behavioural therapy, interpersonal therapy and supportive therapy can be used as first-line treatments for MDD [4, 5]. Up to 30% of MDD patients do not benefit from those treatment options [6]. Depressive patients are considered treatment-resistant when two consecutive trials of treatment with two different psychopharmacological classes, with adequate dose and duration, fail to induce a clinically relevant response [7]. For those treatment-resistant patients electroconvulsive therapy (ECT) can be an effective option [8].

Electroconvulsive therapy

ECT is an effective and safe treatment option for patients with various psychiatric disorders such as depressive, bipolar, primarily psychotic and catatonic disorders [9, 10]. During every ECT session, generalised seizures are induced by a train of short rectangular electrical pulses applied via two surface electrodes while the patient is under general anaesthesia and temporally paralysed. After ECT induced seizures patients often experience postictal side effects such as cognitive deficits and headache [11].

ECT parameters

For ECT, several options for electrode placements can be utilised, with right unilateral (RUL) and bifrontotemporal (BL) electrode placements being the most common in daily practice [12, 13], see Figure 1. Initially, supra-threshold dosed unilateral ECT over the non-dominant hemisphere (mostly right, in rare cases left) is commonly used in The Netherlands because of the lower chance of cognitive side effects and high efficacy. BL electrode placement induces the most generalised seizure with the highest efficacy and more cognitive impairments compared to unilateral ECT [14, 15]. BL ECT is usually utilised in urgent cases whereby quick efficacy is required.

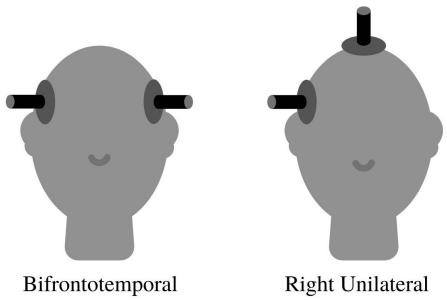

Figure 1: The two most common electrode placements [16].

The coherence between the different stimulus parameters (i.e., energy, electric charge, pulse width, frequency, train duration and amplitude) determines the efficacy and side effects of ECT. In general, the frequency of ECT sessions is twice a week in The Netherlands because the therapeutic effect is comparable with a frequency of three times a week [17–19] and fewer cognitive side effects are seen [18]. In case of severe suicidality or life-threatening catatonic features, up to daily ECT sessions may be executed.

The postictal state

Clinical symptoms

The postictal state is defined as a temporary brain condition following spontaneous or ECT induced seizures. It may involve sensory, cognitive and motor deficits and/or psychiatric symptoms varying in severity. Postictal symptoms can last minutes to days. Examples are postictal anterograde and retrograde amnesia, headache, nausea, delirium and psychosis [20–23]. After complete ECT, most patients suffer from more or less cognitive side effects, which may persist for weeks to months. For both patients and their relatives, the burden of ECT increases with the severity of the postictal symptoms after the sessions and/or cognitive impairments after the course. Although postictal symptoms are extensively described [11, 21, 22, 24], the underlying pathophysiology is not yet fully understood.

Postictal hypoperfusion hypothesis

Farrell et al. [25, 26] hypothesised that the behavioural impairments seen in the postictal state could be explained by long-lasting and severe hypoxia in the brain. This hypothesis is based on the striking similarity between the symptoms expressed by patients in the postictal state and patients with transient hypoxic/ischaemic attacks earlier described by others [22, 27, 28].
A significant decrease in local blood flow and partial oxygen pressure was found in rodents lasting more than an hour after both evoked and spontaneous seizures. The most severe hypoxia occurred 20 to 60 minutes post seizure. To understand the underlying mechanisms, epilepsy-like activity was induced in acute rodent's brain slices *in vitro* to observe vasoconstriction of arterioles more directly. The shift in blood perfusion measured in vivo corresponded with the observed extent of vasoconstriction *in vitro* [25].
In an attempt to reduce the observed vasoconstriction and thus hypoxia in rodents, the researchers used cyclooxygenase-2 (COX-2) and L-type calcium channel antagonists, which both induce vasodilatation. Both drugs were administered before seizure onset, resulting in a reduction in hypoperfusion and hypoxia. It was hypothesised that the enzyme COX-2 which has a proven role in neurovascular coupling [29, 30], also mediates postictal hypoperfusion. Downstream the pathway of cerebral vasoconstriction, it was expected that L-type calcium channels would be activated as a response to COX-2 activation and thereby sustained the hypoperfusion. Blocking this pathway before seizure onset with COX-2-inhibitors, acetaminophen and nimodipine (calcium-antagonist) on different levels in rodents prevented vasoconstriction and thereby severe postictal hypoperfusion and hypoxia. They found that postictal motor weakness and memory loss could both be assigned to hypoperfusion and hypoxia by relieving these symptoms in rodents after administration of nimodipine and acetaminophen, respectively. Seizure duration was not altered by the utilised substances indicating that effects on hypoperfusion and hypoxia could solely be attributed to neurovascular processes.
The relationship between seizures and hypoperfusion was also demonstrated in humans. Ten epilepsy patients were included and underwent perfusion weighted imaging after 24 seizure-free hours (baseline) and one hour after a spontaneous seizure. Postictal hypoperfusion was observed in eight out of ten patients. Based on this work the postictal hypoperfusion hypothesis was validated in both rodents and humans.

Pseudo continuous arterial spin labelling magnetic resonance imaging

Arterial spin labelling magnetic resonance imaging (ASL MRI) is a technique that measures perfusion, also called cerebral blood flow (CBF), in a specific body part. CBF is a measure of blood volume flowing through a point in the brain vasculature, per unit time [31]. Typically quantified in millilitres of blood per 100 gram tissue per minute (ml/100g/min). ASL MRI is based on magnetically labelling the arterial blood water and thereby creating contrast between static tissue and the arterial blood flow.
For acquisition, two types of images in the same region of interest (ROI) are generated, the control images and tagged or labelled images. The signal of static tissue is identical in both images whereas the signal of labelled blood flowing into the ROI is different [32]. To generate the labelled images radiofrequency (RF) pulses are applied to a tissue slab proximal from the ROI to invert or saturate protons, hereby magnetically labelling all protons in the slab [33–35]. The labelled blood protons will flow from the labelling slab towards the ROI and lower the magnetisation equilibrium of the static surrounding tissue with approximately 1-2% [36, 37]. A perfusion-weighted image is generated by pairwise subtraction of label and control images leaving only the signal from the labelled blood protons [38, 39]. Voxel values in a perfusion-weighted image reflect the perfusion per voxel but do not provide an absolute measure of perfusion. The kinetics of ASL are

utilised to transform the perfusion-weighted image into a CBF map with quantitative voxelwise measures of perfusion. Because only a small part of the total signal comprises of labelled blood protons the signal to noise ratio (SNR) is low. To increase SNR, multiple label-control pairs are generated and averaged.
Pseudo continuous (pC)ASL is a preparation module or so-called labelling module, which is a hybrid form of the continuous ASL and the pulsed ASL. In pCASL, the relatively long labelling period comprising of multiple short RF-pulses takes 1-2 s in total [40]. During that period all blood passing the labelling plane is continuously inverted. As a result, all labelled protons arrive in the ROI with approximately the same amount of T_1 decay. Control images are acquired when the phase of every other pulse in the pCASL pulse train is shifted by 180° and the effect of inverting is diminished.

Arterial transit time and post labelling delay
The time it takes magnetically labelled blood water to flow from the labelling region to the blood vessels in the ROI is called the arterial transit time (ATT). This is a physiological parameter varying between individuals, regions and between healthy and pathological tissue [34, 41]. Accurate CBF quantification depends on ATT and not accounting for the differences in ATT amongst patients results in less accurate results [40, 42–45]. The post labelling delay (PLD) is an image acquisition parameter defined as the time between the end of the labelling pulse and the start of image acquisition [43]. Because the ATT changes with age the PLD should be adjusted accordingly. The recommended PLD's for paediatric, adult and geriatric (age > 70) clinical populations are respectively 1500 ms, 1800 ms and at least 2000 ms [40, 46].
Quantification of CBF is most reliable when the PLD is chosen just longer than the longest ATT present in the patient. In that case, all labelled blood water will be delivered to the imaging slice before acquisition thereby avoiding bias by unfinished delivery. Nevertheless, the signal of labelled blood water decays with a time constant T_1, while labelled blood water already represents a small part of the total signal. To assure an acceptable SNR and adequate measure of CBF, a compromise should be made between capturing the signal of all labelled blood water and signal loss because of T_1-decay [46].

Study goals

The goal of this thesis is to gain more understanding about the influence of ECT on CBF and vice versa. The focus lies on ASL-based CBF values, measured at different time points before and after generalised seizures, in MDD patients treated with ECT. In Chapter 1, we aim to calculate reliable global (g)CBF values in ECT patients based on both raw ASL data and CBF maps made by built-in scanner software. Several pre- and post-processing steps will be combined into an imaging pipeline. In Chapter 2, we study the postictal (hypo)perfusion within one hour of an ECT induced seizure. Both postictal gCBF and regional (r)CBF will be compared to baseline thereby evaluating the immediate effect of ECT on the CBF. In Chapter 3, we study the possible associations between the clinical effect of the ECT quantified with the Hamilton Rating Scale for Depression (HRSD)-score and the alterations in gCBF and rCBF in predefined regions.

References

[1] L. Andrade, J.J. Caraveo-anduaga, P. Berglund, R. V. Bijl, R. de Graaf, and W. Vollebergh. The epidemiology of major depressive episodes: results from the international consortium of psychiatric epidemiology (icpe) surveys. *International Journal of Methods in Psychiatric Research*, 12:3–21, 2 2003. https://doi.org/10.1002/mpr.138.
[2] L. Gutiérrez-Rojas, A. Porras-Segovia, H. Dunne, N. Andrade-González, and J. A. Cervilla. Prevalence and correlates of major depressive disorder: a systematic review. *Revista brasileira de psiquiatria (Sao Paulo, Brazil : 1999)*, 42:657–672, 2020.
[3] American Psychiatric Association. *Diagnostic and Statistical Manual of Mental Disorders, Fifth Edition*. 2013.
[4] R. Thom, D. A. Silbersweig, and R. J. Boland. Major depressive disorder in medical illness: A review of assessment, prevalence, and treatment options. *Psychosomatic Medicine*, 81, 2019.
[5] Health Quality Ontario. Psychotherapy for major depressive disorder and generalized anxiety disorder: A health technology assessment. *Ontario health technology assessment series*, 17:1–167, 11 2017.
[6] K. S. Al-Harbi. Treatment-resistant depression: therapeutic trends, challenges, and future directions. *Patient preference and adherence*, 6:369–388, 2012.
[7] D.H. Jaffe, B. Rive, and T.R. Denee. The humanistic and economic burden of treatment-resistant depression in europe: a cross-sectional study. *BMC Psychiatry*, 19:247, 2019.
[8] W. W. van den Broek, T. K. Birkenhäger, D. de Boer, J. P. Burggraaf, B. van Gemert, and T. H.N. Groenland. *Richtlijn Elektroconvulsietherapie*. De Tijdstroom, second edi edition, 2010.
[9] B. Verwey, J. B. Zantvoord, and J. A. Van Waarde. Indicaties en effectiviteit bij overige stoornissen, 2019.
[10] B. Verwey and J. A. Van Waarde. Indicaties en effectiviteit bij stemmingsstoornissen, 2019.
[11] J. C. M. Pottkämper, J. Hofmeijer, J. A. van Waarde, and M. J. A. M. van Putten. The postictal state — what do we know? *Epilepsia*, n/a, 5 2020. doi: 10.1111/epi.16519.

[12] C.H. Kellner, J. Obbels, and P. Sienaert. When to consider electroconvulsive therapy (ect). *Acta Psychiatrica Scandinavica*, 141:304–315, 4 2020. doi: 10.1111/acps.13134.
[13] H. P. Spaans, P. Sienaert, and J. A. Van Waarde. Elektrodeplaatsing, stimulusparameters, insultdrempel en doseringsstrategie, 2019.
[14] W. H. Lee, Z. D. Deng, T. S. Kim, A. F. Laine, S. H. Lisanby, and A. V. Peterchev. Regional electric field induced by electroconvulsive therapy in a realistic finite element head model: Influence of white matter anisotropic conductivity. *NeuroImage*, 59:2110–2123, 2012.
[15] D. M. Martin, V. Gálvez, and C. K. Loo. Predicting retrograde autobiographical memory changes following electroconvulsive therapy: Relationships between individual, treatment, and early clinical factors. *The international journal of neuropsychopharmacology*, 18, 6 2015.
[16] S. Surya and N. Mori. Recent literature on electroconvulsive therapy techniques for the treatment of depression. *The American Journal of Psychiatry Residents' Journal*, 10:3–5, 3 2015.
[17] F. Charlson, D. Siskind, S. A. R. Doi, E. McCallum, A. Broome, and D. C. Lie. Ect efficacy and treatment course: a systematic review and meta-analysis of twice vs thrice weekly schedules. *Journal of affective disorders*, 138:1–8, 4 2012.
[18] B. Shapira, N. Tubi, and B. Lerer. Balancing speed of response to ect in major depression and adverse cognitive effects: role of treatment schedule. *The journal of ECT*, 16:97–109, 6 2000.
[19] W. Chanpattana. Seizure threshold in electroconvulsive therapy: Effect of instrument titration schedule. *German J Psychiatry*, 4, 1 2001.
[20] R. S. Fisher and S. C. Schachter. The postictal state: a neglected entity in the management of epilepsy. *Epilepsy behavior : EB*, 1:52–59, 2 2000.
[21] A. Subota, S. Khan, C. B. Josephson, S. Manji, S. Lukmanji, and P. Roach. Signs and symptoms of the postictal period in epilepsy: A systematic review and meta-analysis. *Epilepsy behavior : EB*, 94:243–251, 5 2019.
[22] J. Rémi and S. Noachtar. Clinical features of the postictal state: Correlation with seizure variables. *Epilepsy Behavior*, 19:114–117, 2010.
[23] A. M. Kanner, M. Trimble, and B. Schmitz. Postictal affective episodes. *Epilepsy behavior : EB*, 19:156–158, 10 2010.
[24] G. Krauss and W. H. Theodore. Treatment strategies in the postictal state. *Epilepsy behavior : EB*, 19:188–190, 10 2010.
[25] J. S. Farrell, I. Gaxiola-Valdez, M. D. Wolff, L. S. David, H. I. Dika, and B. L. Geeraert. Postictal behavioural impairments are due to a severe prolonged hypoperfusion/hypoxia event that is cox-2 dependent. *eLife*, 5:e19352, 11 2016.
[26] J. S. Farrell, R. Colangeli, M. D. Wolff, A. K. Wall, T. J. Phillips, and A. George. Postictal hypoperfusion/hypoxia provides the foundation for a unified theory of seizure-induced brain abnormalities and behavioral dysfunction. *Epilepsia*, 58:1493–1501, 9 2017. doi: 10.1111/epi.13827.
[27] P. Vilela. Acute stroke differential diagnosis: Stroke mimics. *European Journal of Radiology*, 96:133–144, 2017.
[28] F. Scheperjans, H. Silvennoinen, S. Mustanoja, M. Palomäki, and N. Forss. Hypoperfusion of an entire cerebral hemisphere - stroke or postictal deficit? *Case reports in neurology*, 3:233–238, 9 2011.
[29] C. Lecrux, X. Toussay, A. Kocharyan, P. Fernandes, S. Neupane, and M. Lévesque. Pyramidal neurons are "neurogenic hubs" in the neurovascular coupling response to whisker stimulation. *The Journal of neuroscience : the official journal of the Society for Neuroscience*, 31:9836–9847, 7 2011.
[30] A. Lacroix, X. Toussay, E. Anenberg, C. Lecrux, N. Ferreirós, and A. Karagiannis. Cox-2-derived prostaglandin e2 produced by pyramidal neurons contributes to neurovascular coupling in the rodent cerebral cortex. *The Journal of neuroscience : the official journal of the Society for Neuroscience*, 35:11791–11810, 8 2015.
[31] A. C. Guyton. *Basic human physiology: normal function and mechanisms of disease*. Saunders, 1971.
[32] E. T. Petersen, T. Lim, and X. Golay. Model-free arterial spin labeling quantification approach for perfusion mri. *Magnetic resonance in medicine*, 55:219–232, 2 2006.
[33] R. L. Wolf and J. A. Detre. Clinical neuroimaging using arterial spin-labeled perfusion magnetic resonance imaging. *Neurotherapeutics : the journal of the American Society for Experimental NeuroTherapeutics*, 4:346–359, 7 2007.
[34] E. T. Petersen, I. Zimine, Y. C. L. Ho, and X. Golay. Non-invasive measurement of perfusion: a critical review of arterial spin labelling techniques. *The British Journal of Radiology*, 79:688–701, 8 2006. doi: 10.1259/bjr/67705974.
[35] D. S. Williams, J. A. Detre, J. S. Leigh, and A. P. Koretsky. Magnetic resonance imaging of perfusion using spin inversion of arterial water. *Proceedings of the National Academy of Sciences of the United States of America*, 89:212–216, 1 1992.
[36] A. D. (Mallinckrodt Institue of Radiology/ Washington University of Medicine) Ester. Arterial spin labeling (asl) - what is asl and how does it work?
[37] X. Golay, J. Hendrikse, and T. C. C. Lim. Perfusion imaging using arterial spin labeling. *Topics in Magnetic Resonance Imaging*, 15, 2004.
[38] J. M. Pollock, H. Tan, R. A. Kraft, C. T. Whitlow, J. H. Burdette, and J. A. Maldjian. Arterial spin-labeled mr perfusion imaging: clinical applications. *Magnetic resonance imaging clinics of North America*, 17:315–338, 5 2009.
[39] S. Petcharunpaisan, J. Ramalho, and M. Castillo. Arterial spin labeling in neuroimaging. *World journal of radiology*, 2:384–398, 10 2010.
[40] W. Dai, D. Garcia, C. de Bazelaire, and D. C. Alsop. Continuous flow-driven inversion for arterial spin labeling using pulsed radio frequency and gradient fields. *Magnetic Resonance in Medicine*, 60:1488–1497, 12 2008. https://doi.org/10.1002/mrm.21790.
[41] R. P. H. Bokkers, H. B. van der Worp, W. P. T. M. Mali, and J. Hendrikse. Noninvasive mr imaging of cerebral perfusion in patients with a carotid artery stenosis. *Neurology*, 73:869–875, 9 2009.
[42] T. Tsujikawa, H. Kimura, T. Matsuda, Y. Fujiwara, M. Isozaki, and K. I. Kikuta. Arterial transit time mapping obtained by pulsed continuous 3d asl imaging with multiple post-label delay acquisitions: Comparative study with pet-cbf in patients with chronic occlusive cerebrovascular disease. *PLOS ONE*, 11:e0156005, 6 2016.
[43] D. C. Alsop and J. A. Detre. Reduced transit-time sensitivity in noninvasive magnetic resonance imaging of human cerebral blood flow. *Journal of Cerebral Blood Flow Metabolism*, 16:1236–1249, 11 1996. doi: 10.1097/00004647-199611000-00019.
[44] P. Bladt, M. J. P. van Osch, P. Clement, E. Achten, J. Sijbers, and A. J. den Dekker. Supporting measurements or more averages? how to quantify cerebral blood flow most reliably in 5 minutes by arterial spin labeling. *Magnetic Resonance in Medicine*, 84:2523–2536, 11 2020. https://doi.org/10.1002/mrm.28314.
[45] M. J. P. van Osch, W. M. Teeuwisse, Z. Chen, Y. Suzuki, M. Helle, and S. Schmid. Advances in arterial spin labelling mri methods for measuring perfusion and collateral flow. *Journal of cerebral blood flow and metabolism : official journal of the International Society of Cerebral Blood Flow and Metabolism*, 38:1461–1480, 9 2018.
[46] D. C. Alsop, J. A. Detre, X. Golay, M. Günther, J. Hendrikse, and L. Hernandez-Garcia. Recommended implementation of arterial spin-labeled perfusion mri for clinical applications: A consensus of the ismrm perfusion study group and the european consortium for asl in dementia. *Magnetic resonance in medicine*, 73:102–116, 1 2015.

General methods

Study population and study design

The current study data were acquired as part of the clinical trial SYNAPSE: Study of the effect of Nimodipine and Acetaminophen on Postictal Symptoms after ECT. Within the SYNAPSE it is investigated whether the administration of the vasodilatory drugs nimodipine and acetaminophen before the ECT session can relieve postictal symptoms. Postictal manifestations after both ECT induced seizures and spontaneous seizures in epilepsy patients are similar in terms of electroencephalographic and clinical characteristics [1]. Therefore, ECT patients are included in the SYNAPSE and served as a human model to study the postictal state in a controlled way. Prior to each ECT session, either nimodipine, acetaminophen or a placebo (i.e., a glass of water) was administered in a random and counterbalanced way. Because patient inclusion in the SYNAPSE is still ongoing, the interventions remained blinded and played no role in this thesis.
Patients were included in the SYNAPSE if they had a current clinical diagnosis of depressive episode, were older than 17 years and were able to give written informed consent. When potential patients had a known allergy to acetaminophen or nimodipine, met contraindications for MRI or electroencephalogram (EEG) or used acetaminophen, calcium-antagonists or nonsteroidal anti-inflammatory drugs in a chronic way that could not be interrupted during the two days leading up to the ECT session, they were excluded from the study. All patients in the SYNAPSE were treated in Rijnstate hospital.
Included patients underwent six MRI scans. The first MRI scan was acquired before the start of the first ECT session (baseline), three consecutive scans were made within one hour after an ECT induced seizure (postictal) and the last two scans were made within two weeks after the last ECT session (end-ECT) and around three months thereafter (follow-up).

ECT procedure

ECT was carried out while the patient was under short-lasting general anaesthesia induced with etomidate, connected to non-invasive ventilation, and paralysed after administration of succinylcholine. The initial seizure threshold was determined during the first ECT session with stimulus dose titration.
The electrical current was administered by a trained psychiatrist while an anesthesiologist and assistant monitored the patient's vital signs. Approximately one minute after the ECT-stimulus, the seizure ceases and several minutes later the patient awakens [2]. In case of severe postictal confusion and agitation, additional drugs were administered such as propofol, haloperidol, lorazepam, diazepam or midazolam. In our study population, RUL and BL electrode placement were used most often, while one patient was treated with left unilateral (LUL) electrode placement.
Every patient received ECT twice a week with at least one day between both sessions. The number of ECT sessions was variable between patients and dependent on treatment response and the occurrence and severity of postictal symptoms. In some patients, the frequency of ECT sessions was lowered to once a week, after completion of the index ECT course. In that case, the end-ECT MRI was acquired after completion of the index ECT course.

References

[1] Julia C M Pottkämper, Joey P A J Verdijk, Jeannette Hofmeijer, Jeroen A van Waarde, and Michel J A M van Putten. Seizures induced in electroconvulsive therapy as a human epilepsy model: A comparative case study. *Epilepsia Open*, n/a, 8 2021. https://doi.org/10.1002/epi4.12532.

[2] M. Grözinger, E. S. Smith, and A. Conca. On the significance of elektroconvulsive therapy in the treatment of severe mental diseases. *Wiener klinische Wochenschrift*, 127:297–302, 2015.

1 Calculation of global CBF values based on raw arterial spin labelling data and CBF maps generated by Philips software

1.1 Introduction

Several imaging modalities are suitable for measuring CBF such as single-photon emission computed tomography (SPECT), positron emission tomography (PET), blood oxygen level dependent (BOLD) functional (f)MRI and ASL MRI. With BOLD fMRI an indirect estimate of brain function is obtained based on relative metrics [1, 2]. Both SPECT and PET require the use of radioactive tracers and spatial resolution is poor in comparison with ASL MRI [2]. Therefore, ASL MRI was considered best suited for measuring CBF in this study.
Various parameters and protocol choices within the ASL acquisition play a role in the quantification of CBF values. Several readout schemes, labelling methods and quantification models are available next to the possibility to adjust parameters such as PLD and the number of background suppression pulses. A consensus paper, also referred to as the 'White-paper' [3], developed by the perfusion study group of the International Society for Magnetic Resonance in Medicine in collaboration with the European consortium for ASL in dementia was introduced to stimulate uniformity. The 'White-paper' provided a go-to methodology for the implementation of ASL MRI in the clinical setting and included a deliberately simplified model and parameter choices [4]. Several studies that adopted the recommendations showed CBF estimates similar to the values obtained with the gold standard ^{15}0-PET [5–7].
Although the consensus statement offers a reliable methodology for quantification of pCASL data in clinical practice, several sources of error interfere with robust quantification. First, specific parameters within the simplified model were fixed to values known in literature, whereas those parameters may vary in reality. Secondly, the consensus model is an oversimplification of the fundamental perfusion mechanisms [4]. The kinetic model from Buxton et al. [8] can be utilised to get closer to physiological correct CBF values. Moreover, the process of CBF and the effects of several ASL acquisition parameters on the quantification thereof has been a topic of interest. [4, 9–11]. This knowledge can be utilised to get closer to more robust CBF quantification.
CBF maps can be generated directly after ASL data acquisition with incorporated MRI scanner software. The built-in software is partly a black-box due to the patented software syntax. Therefore, it is not known how this map was created exactly and which parameters were included. The built-in algorithms are very fast, and therefore easy to use in clinical practice. A CBF map can also be generated based on raw ASL data and image processing software, which is time-consuming but precise.
The aim of the current study is to generate an automated imaging pipeline by using FSL software to calculate reliable gCBF values. Based on both raw pCASL data and CBF maps based on built-in Philips Ingenia software.

1.2 Methods

1.2.1 Study population and study design

For a description of the study population and study design, we refer to the subsection 'Study population and study design' in the general methods on page 9 of this thesis.

1.2.2 MRI acquisition

The Philips Ingenia 3T MRI scanner (Philips Healthcare, Best, The Netherlands) with a 15-channel head coil was utilised to acquire ASL images and T_1-weighted anatomical images. Three-dimensional (3D) T_1-weighted images were acquired with an isotropic voxel size of 1.1 mm, a repetition time (TR) and echo time (TE) of respectively 7.5 ms and 4.6 ms, a field of view of 256 x 238 x 159.5 mm and consisting of 145 sagittal slices. The single delay ASL images were acquired with a pseudo-continuous inversion module, 3D gradient-and-spin-echo (GRASE) readout module, labelling duration of 1800 ms, in line with the 'White-paper' [3], PLD of 1900 ms, voxel size of 3 x 3 x 6 mm, field of view of 240 x 240 x 126 mm and consisting of 21 transverse slices. A 3D-readout module was utilised because it is less sensitive to movement artefacts. Normalisation was applied by using four background suppression pulses to enable CBF quantification. The raw pCASL data

consisted of five dynamics, whereof one dynamic served as a 3D calibration image. This calibration volume is a proton density-weighted image with relatively long TR used to correct for the equilibrium magnetisation of arterial blood.

1.2.3 Data structure

For pre-processing, MRI data were sorted with a DICOM sorting utility part of Python programming language (version 3.8). The data were structured per patient and MRI session according to the Brain imaging data structure (BIDS) format (sub-identifier/ses-identifier/data) [12]. The resulting DICOM data were converted into the NifTI format to enable working with FSL 6.0.3 (FMRIB Software Library v6.0.3, Analysis Group, FMRIB, Oxford, United Kingdom).

1.2.4 MRI spaces

Brain MRI scans were acquired in different spaces. The space in which the ASL image was acquired is called the native space. Anatomical images, also called structural images, were acquired in the structural space. The voxel size and field of view differ per MRI space. The voxel size of pCASL images was bigger compared to structural images which makes it impossible to do voxel-based post-processing and analyses. To enable comparison of different types of images and group analyses, images were registered to a general coordinate system. Therefore, the MNI152 template [13] was utilised, also known as standard space. This coordinate system created by group-wise registration of 152 healthy adults includes both structural and functional information.

1.2.5 Registration

Image registration is a method to align multiple images to obtain spatial correspondence of anatomical structures. Two kinds of registration algorithms can be distinguished: linear and non-linear registration algorithms. The FSL function FLIRT [14, 15] was utilised for linear registration and FNIRT and APPLYWARP [16] for non-linear registration. Affine transformations were utilised for the linear registration. Affine transformations involve rotation, translation, scaling and shearing along the x-, y-, and z-axis resulting in twelve degrees of freedom. Linear registration is a global registration. On the other hand, non-linear registration can model local deformations and has a higher degree of elasticity. One can think of non-linear registration as squeezing your image matrix like a sponge: some parts deform a lot while other parts stay the same. In this registration-based image analysis, linear registration served as an essential first step and was followed by non-linear registration. Output from the linear registration was needed to feed the non-linear registration algorithm [17].

1.2.6 Assessment of global grey matter CBF

For the assessment of the global brain perfusion only grey matter (GM) voxels were utilised in the current study. The PLD of 1900ms utilised in this study is better applicable for GM CBF assessment. Due to lower blood flow, the ATT in deep white matter (WM) can be 2000ms or longer causing low SNR in WM [3]. Moreover, GM ASL signal can easily overrule the WM signal in both in-plane or through-plane directions [18]. Therefore, the use of pCASL for the detection of WM CBF deficits is considered too insensitive for clinical applications [19], and only GM CBF will be used. Henceforth, the term CBF in this thesis will refer to GM CBF only.

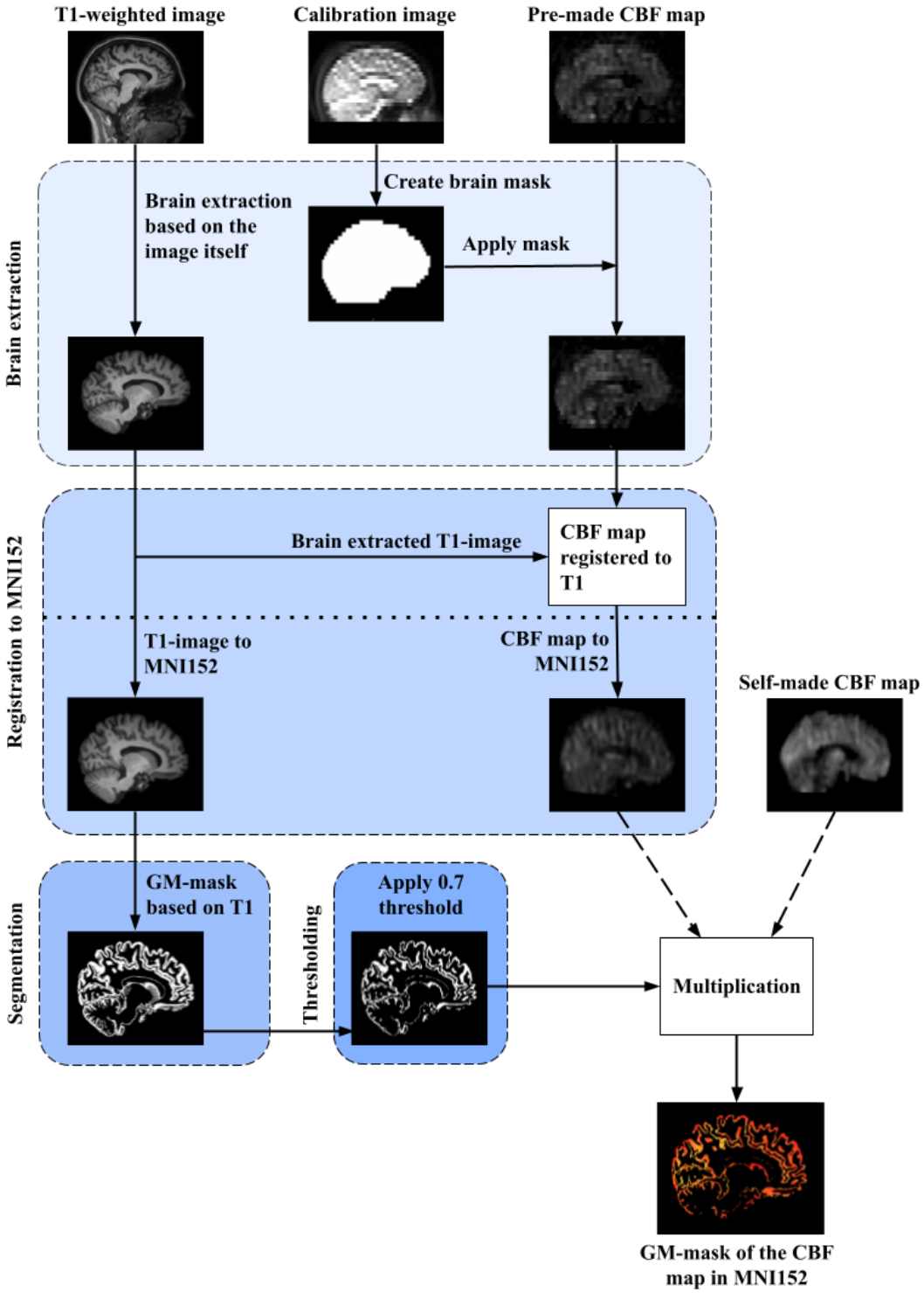

Figure 2: Post-processing pipeline for both the CBF maps. For the pre-made CBF-map the whole pipeline is applicable. Processing of the self-made CBF map starts from the dotted line. The dotted arrows pointing to 'multiplication' indicate that either the pre-made or self-made CBF map can serve as input. The first block involves brain extraction, where after both the T_1-weighted image and the pre-made CBF map were registered to standard space. The self-made CBF map was already in standard space. The T_1-weighted image was utilised to segment the GM voxels and make a GM probability mask. After thresholding, this mask was multiplied with the CBF map (self-made or pre-made) in standard space to segment the GM-voxels.

1.2.7 Calculation of the grey matter CBF

Command-line tools from FSL version 6.0.3 and Python version 3.8 were utilised to create an imaging pipeline and algorithms in Atom version 1.48.0 on a Linux based system. Two types of CBF maps were utilised in the current study. The first type was created based on raw pCASL data using functions from BASIL [20] part of FSL. Henceforward, these CBF maps will be referred to as self-made CBF maps. The steps taken to make the self-made CBF maps are visualised in Figure 3. The five dynamics of the pCASL data were split into the calibration volume and four label-control pairs. Secondly, the labelled images were subtracted from the control images to create perfusion images. A mean perfusion image was made by taking the average of the four created perfusion images. To convert the generated perfusion image into a CBF map with absolute values, quantification was done with the function oxford_asl that utilises the kinetic model described by Buxton et al. [8]. The input for this function consisted of the mean perfusion image, calibration image, several scanning parameter choices in accordance with Buxton et al. [8], and the output folder of fsl_anat. The latter function included a pipeline for processing structural images involving brain extraction, cortical and subcortical structure segmentation and registration to standard space. The ATT, T_{1_blood} and T_{1_tissue} were set to 1.3, 1.65 and 1.3 s respectively. The output of oxford_asl consisted of the calibrated CBF maps in native, structural and standard space. Various parameters influenced the CBF values in the resulting maps. The voxel values in the self-made CBF-maps were divided by 0.81 because four background suppression pulses were applied within the Philips pCASL acquisition. The suppression efficiency was assumed to be 95% per pulse in accordance with the built-in Philips software. Therefore, a correction factor of $0.95^4 = 0.81$ was applied to the self-made CBF maps.

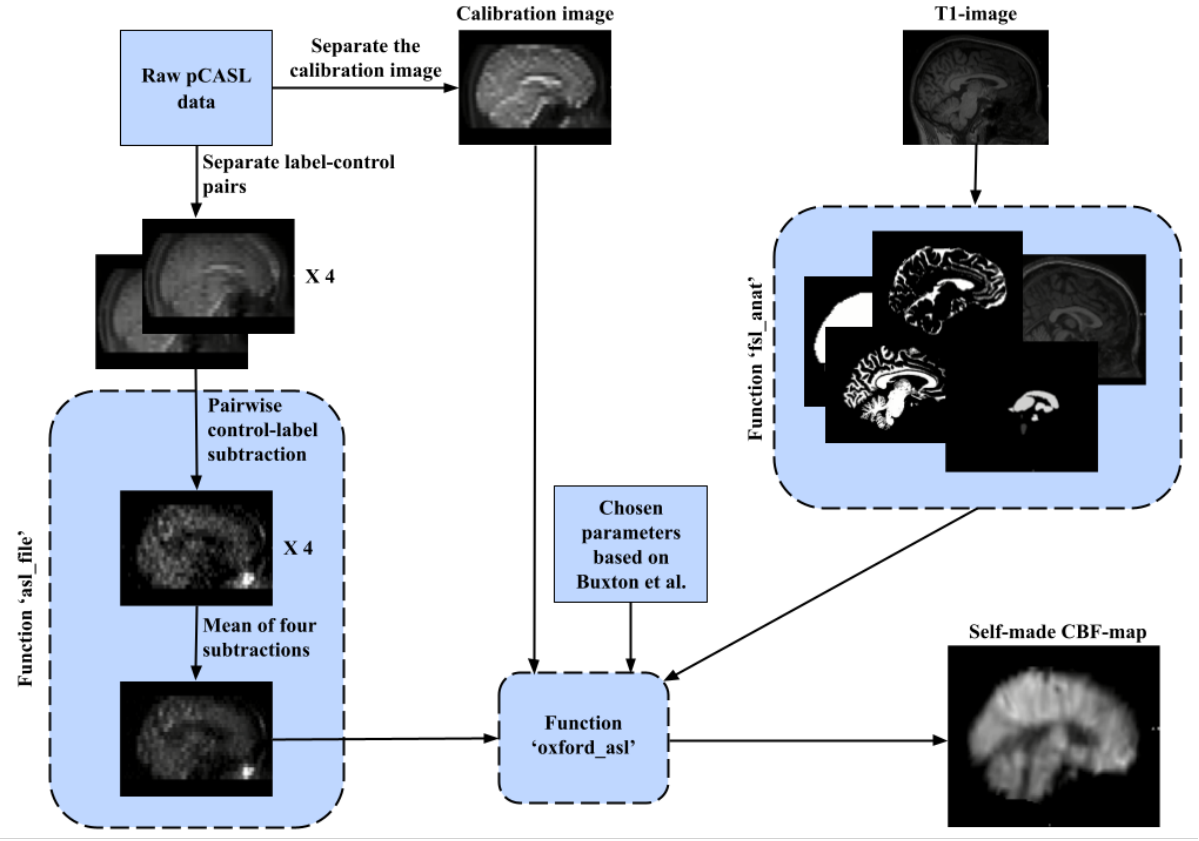

Figure 3: Generation of self-made CBF map based on several FSL functions, T_1-weighted images and raw pCASL data.

The second type of CBF maps were automatically generated by incorporated Philips software and will be referred to as pre-made CBF maps. Those CBF maps were only available in native space.
The pipeline utilised to calculate the GM CBF based on the pre-made and/or self-made CBF map is presented in Figure 2. The part of the pipeline above the dotted line only applies to processing of the pre-made CBF maps because the self-made CBF maps were available in standard space. To register the pre-made CBF map to standard space the raw pCASL data and the structural T_1-weighted images were needed. First, brain extraction was done with the BET (Brain Extraction Tool) from FSL [21], to exclude structures such as dura mater and skull from the images. Due to poor spatial resolution and contrast direct brain extraction of the pre-made CBF map was not possible. The calibration image, which is part of the raw pCASL data, was utilised to create a binary mask that served as input for BET and enabled brain extraction. The resulting brain extracted images were registered to standard space with linear and non-linear registration. For a complete overview of all the registration steps of the different images, we refer to Appendix I on page 47 of this thesis.
After registration GM voxels were segmented from the rest of the brain to enable GM gCBF calculation. Direct segmentation from the CBF map was not possible because the map does not contain structural information and has low resolution. Therefore, segmentation was based on the T_1-weighted images using FAST [22]. One of the outputs of FAST was a probability image. The voxels in the probability image have values between zero and one, indicating the portion of those specific voxels being identified as GM. For a reliable analysis, only voxels with a majority of GM were considered. The probability image was thresholded so that only voxels with a voxel value ≥ 0.7 were included in the binary GM mask [23]. By multiplying the CBF map in standard space with the binary GM mask, a CBF map was created including only GM voxels. The mean value of all the non-zero voxels within that image was calculated to determine the gCBF.

1.3 Results

An imaging pipeline was written that could calculate the gCBF in all patients and for all sessions based on both types of CBF maps. The baseline CBF values of twelve patients based on the pre-made and self-made CBF maps are provided in Table 1. For some patients in this study, the absolute values for gCBF were low in comparison with normal quantitative values ranging around 50 ml/100g/min [24–26]. Especially, when the threshold for penumbra is taken into consideration which is around 20 ml/100g/min [24]. Values below 20 ml/100g/min were coloured red in Table 1.
For all patients, the values based on the pre-made CBF map are lower in comparison to the values based on the self-made CBF maps. Absolute differences range between 1.12 and 16.29 ml/100g/min. CBF values based on self-made CBF maps were on average 22.3% (SD $\pm$ 4.34%, min = 7.95%, max = 32.68%) lower compared to the values based on pre-made CBF maps.

Table 1: gCBF values per patient at baseline in ml/100g/min based on the self-made and pre-made CBF maps. Values below 20 ml/100g/min are coloured in red because they indicate severe hypoperfusion.

	Pre-made CBF map	Self-made CBF map
sub-001	30.51	40.45
sub-003	23.90	30.70
sub-004	47.83	63.30
sub-006	31.49	41.29
sub-007	28.47	38.83
sub-008	46.98	62.38
sub-009	36.97	45.27
sub-011	14.82	18.63
sub-012	37.36	48.30
sub-013	36.38	46.02
sub-018	38.44	52.55
sub-020	17.99	22.68

1.4 Discussion

An automatic imaging pipeline was written to calculate gCBF values per patient and MRI session based on both raw ASL data and pre-made CBF maps, after a few steps of pre-processing. The baseline gCBF values based on the raw ASL data in this group of severely depressed patients lay within the normal physiological range with exception of a few low values. Whereas the values based on the pre-made scan were approximately 20% lower.

Low gCBF values based on both self-made and pre-made CBF maps
Most of the determined baseline CBF values of our patient group lay within the normal physiological range [24–26]. Nevertheless, the absolute values for baseline gCBF exceeded the threshold for penumbra in some severely depressed patients. These low values tended to be consistent in patients across the other sessions. The low values could not be explained by known vascular abnormalities. Although our patients were severely depressed, none of these patients were identified as having severe neurological dysfunctions (e.g. altered consciousness, paralysis, aphasia). After a thorough post-analysis of the effect of several parameters such as calibration method, use of averaged calibration images, scaling factors within dcm2niix, and correction factors for inversion efficiency of the labelling process it was concluded that the problem did not stem from the made imaging pipeline. Moreover, imaging protocols and results were validated by an independent research group aft the University of Leiden.
The found absolute CBF values are, next to the made algorithm, also dependent on assumptions within the utilised functions and choices for scanner parameters. Within the function oxford_asl, utilised to create self-made CBF maps, a fixed value for the longitudinal relaxation time of blood T_1_blood was used. But the value of T_1_blood is susceptible to fluctuations in factors defining the physiological state of blood such as hematocrit, oxygenation and blood cell pathology's [27–29]. Next to that, the labelling efficiency α was fixed at 0.85 in accordance with Alsan et al. [10]. α can differ between arteries, patients and MRI sessions depending on magnetic field inhomogeneities, planning of the labelling plane and blood flow velocity [30, 31]. The discrepancy between the fixed parameter values in oxford_asl and physiological values in the patient may result in a CBF quantification bias [4].
Secondly, one of the scanner parameters prone to be a confounder in the quantification process is the PLD. As discussed before, a PLD of 1900ms was chosen although elderly patients (for which a PLD of 2000ms is recommended) were included in the study as well. Three out of twelve patients were >60 years of age and two of them showed extremely low gCBF baseline values. Therefore, it is likely that part of the labelled blood water did not arrive in the ROI before acquisition resulting in a lower gCBF and arterial artefacts.
The resulting gCBF values are calculated based on a robust algorithm and validated by an independent research group. Due to a certain combination of the discussed confounders, errors in gCBF quantification can occur in varying degrees. This may explain the found unrealistic low values in patient sub-009, sub-011 and sub-020, without clinical neurological symptoms.

Difference between self-made and pre-made CBF values
On average the gCBF values determined based on the self-made CBF maps were 22.3% higher compared to the values based on pre-made CBF maps. Although both the pre-made and self-made CBF maps were generated based on Buxton et al. [8] voxel values in the self-made CBF maps are already higher in the unregistered images. This argues for a difference in Philips' CBF quantification and not a difference originating from the in-house developed algorithms. There are a few dissimilarities between the Philips software and the code made for the self-made CBF maps. First of all, the calibration image is smoothed and corrected for incomplete longitudinal relaxation (T_1) in the Philips software. Also, in the Philips software a T_1_tissue of 1100 ms was utilised instead of the 1350 ms which was proposed in the 'White-paper' [19], and implemented in the self-made CBF-images. It is not known to what extent these differences can explain the discrepancy between both CBF maps. The Philips software is designed for radiologists and not for precise quantification of the CBF per se. For research purposes it is recommended to create specific code adapted to the explicit research goals.

Strengths and limitations
Establishing CBF based on pCASL is considered a strength of this study. pCASL is a patient-friendly imaging method that does not require the use of radiation nor contrast agents. Moreover, motion artefacts were limited by utilising inflatable cushions to fixate the head of patients. Also, two healthy controls underwent T_1-weighted and pCASL MRI to validate the calculated CBF. Nevertheless, the methods of the current study also included some limitations. A fixed number of 21 slices was utilised for the pCASL acquisition. To fit the whole cortex within the field of view some changes needed to be made during acquisition planning. At the start of SYNAPSE, this was not executed correctly resulting in pCASL images missing the cranial part of the cortex. This was the case for the baseline scan up to and including the end-ECT scan of sub-001, sub-003 and sub-004. In those scans, part of the cortex was not included in the analysis. Another limitation comes with the several variable factors that contribute to and may influence measured CBF values. First of all, the majority of patients was on antidepressants during their participation in the study. Secondly, although patients were restricted from two hours before ECT, several patients frequently used coffee and/or cigarettes resulting in both caffeine and nicotine possibly affecting the measured CBF. Next to that, undergoing ECT is accompanied by administration of several drugs such as succinylcholine, etomidate and benzodiazepines. No significant changes were reported in CBF velocity and cerebral perfusion pressure within fifteen minutes after administration of succinylcholine [32, 33]. Nevertheless, a reduction in gCBF was reported after etomidate and propofol injection [34, 35]. Lastly, also the depressive episode itself leads to changes in CBF [36–41]. Thus, absolute CBF values should be interpreted carefully and utilising CBF values that are normalised with respect to baseline is advised.

Accuracy of pCASL CBF
To improve the accuracy of the calculated absolute CBF values several adjustments can be made to the acquisition protocol. CBF quantification can benefit from performing additional measurements or utilising different forms of the ASL experiment [4].
Instead of choosing literature values the T_1_blood and labelling efficiency can be measured with additional MRI scans [29, 42]. Based on multi-PLD pCASL [43, 44] or time-encoded pCASL [45] the perfusion process can be sampled at multiple time points. Compared to single-PLD pCASL those techniques allow for more accurate CBF measurements and ATT quantification. Nevertheless, these adjustments take time. When keeping the total acquisition time constant, implementing these adjustments will limit the number of acquired label-control pairs and thereby the precision of CBF quantification. Bladt et al. [4] attempted to optimise the distribution of scan time and find the optimal balance between averaging ASL data and performing supporting measurements. They concluded that it is beneficial to spend part of the scan-time on measuring the labelling efficiency and T_1_blood in the general population. The tagging efficiency in pCASL, which is the phase difference between control and labelled images, could be a source of quantification error [11]. At the tagging location pCASL can be sensitive to off-resonance fields and gradient imperfections [46]. To overcome this problem, Jung et al. [11] used a robust prescan procedure with a 7T MRI scanner. The resulting CBF values were more consistent compared to values obtained with flow-sensitive alternating inversion recovery MRI and higher compared to CBF values acquired with conventional pCASL. They concluded that multi-phase pCASL should be utilised in clinical applications when accurate quantitative measures of CBF are required.
Thus compared to the current acquisition protocol several adjustments can improve the reliability of pCASL based CBF values in future research. Even without prolonging the acquisition time.

Conclusion
An imaging pipeline was created to calculate gCBF values based on two types of CBF maps. The gCBF values based on pre-made CBF maps were lower compared to the values based on the self-made CBF maps. We expect the calculated values to be realistic. With the exception of a few values that indicated severe hypoxia in patients who did not show neurological deficits. For the remainder of this thesis, the self-made CBF maps will be utilised in all analyses because it is exactly known how these were established.

References

[1] T. T. Liu and G. G. Brown. Measurement of cerebral perfusion with arterial spin labeling: Part 1. methods. *Journal of the International Neuropsychological Society : JINS*, 13:517–525, 5 2007.

[2] A. M. Leaver, R. Espinoza, T. Pirnia, S. H. Joshi, R. P. Woods, and K. L. Narr. Modulation of intrinsic brain activity by electroconvulsive therapy in major depression. *Biological Psychiatry: Cognitive Neuroscience and Neuroimaging*, 1:77–86, 2016.

[3] D. C. Alsop, J. A. Detre, X. Golay, M. Günther, J. Hendrikse, and L. Hernandez-Garcia. Recommended implementation of arterial spin-labeled perfusion mri for clinical applications: A consensus of the ismrm perfusion study group and the european consortium for asl in dementia. *Magnetic resonance in medicine*, 73:102–116, 1 2015.

[4] P. Bladt, M. J. P. van Osch, P. Clement, E. Achten, J. Sijbers, and A. J. den Dekker. Supporting measurements or more averages? how to quantify cerebral blood flow most reliably in 5 minutes by arterial spin labeling. *Magnetic Resonance in Medicine*, 84:2523–2536, 11 2020. https://doi.org/10.1002/mrm.28314.

[5] K. Zhang, H. Herzog, J. Mauler, C. Filss, T. W. Okell, and E. R. Kops. Comparison of cerebral blood flow acquired by simultaneous [15o]water positron emission tomography and arterial spin labeling magnetic resonance imaging. *Journal of cerebral blood flow and metabolism : official journal of the International Society of Cerebral Blood Flow and Metabolism*, 34:1373–1380, 8 2014.

[6] D. F. R. Heijtel, H. J. M. M. Mutsaerts, E. Bakker, P. Schober, M. F. Stevens, and E. T. Petersen. Accuracy and precision of pseudo-continuous arterial spin labeling perfusion during baseline and hypercapnia: A head-to-head comparison with 15o h2o positron emission tomography. *NeuroImage*, 92:182–192, 2014.

[7] E. Kilroy, L. Apostolova, C. Liu, L. Yan, J. Ringman, and D. J. J. Wang. Reliability of two-dimensional and three-dimensional pseudo-continuous arterial spin labeling perfusion mri in elderly populations: comparison with 15o-water positron emission tomography. *Journal of magnetic resonance imaging : JMRI*, 39:931–939, 4 2014.

[8] R. B. Buxton, L. R. Frank, E. C. Wong, B. Siewert, S. Warach, and R. R. Edelman. A general kinetic model for quantitative perfusion imaging with arterial spin labeling. *Magnetic Resonance in Medicine*, 40:383–396, 1998.

[9] M. J. P. van Osch, W. M. Teeuwisse, Z. Chen, Y. Suzuki, M. Helle, and S. Schmid. Advances in arterial spin labelling mri methods for measuring perfusion and collateral flow. *Journal of cerebral blood flow and metabolism : official journal of the International Society of Cerebral Blood Flow and Metabolism*, 38:1461–1480, 9 2018.

[10] S. Aslan, F. Xu, P. L. Wang, J. Uh, U. S. Yezhuvath, and M. van Osch. Estimation of labeling efficiency in pseudocontinuous arterial spin labeling. *Magnetic resonance in medicine*, 63:765–771, 3 2010.

[11] Y. Jung, E. C. Wong, and T. T. Liu. Multiphase pseudocontinuous arterial spin labeling (mp-pcasl) for robust quantification of cerebral blood flow. *Magnetic Resonance in Medicine*, 64:799–810, 9 2010. https://doi.org/10.1002/mrm.22465.

[12] K. J. Gorgolewski, T. Auer, V. D. Calhoun, R. C. Craddock, S. Das, and E. P. Duff. The brain imaging data structure, a format for organizing and describing outputs of neuroimaging experiments. *Scientific Data*, 3:160044, 2016.

[13] J. Mazziotta, A. Toga, A. Evans, P. Fox, J. Lancaster, and K. Zilles. A probabilistic atlas and reference system for the human brain: International consortium for brain mapping (icbm). *Philosophical transactions of the Royal Society of London. Series B, Biological sciences*, 356:1293–1322, 8 2001.

[14] M. Jenkinson and S. Smith. A global optimisation method for robust affine registration of brain images. *Medical image analysis*, 5:143–156, 6 2001.

[15] M. Jenkinson, P. Bannister, M. Brady, and S. Smith. Improved optimization for the robust and accurate linear registration and motion correction of brain images. *NeuroImage*, 17:825–841, 10 2002.

[16] J. L. R. Andersson, M. Jenkinson, and S. Smith. Non-linear registation, aka spatial normalisation fmrib technical report tr07ja2. *FMRIB Analysis Group of University of Oxford*, 2:e21, 2007.

[17] X. Zhang, Y. Feng, W. Chen, X. Li, A. V. Faria, and Q. Feng. Linear registration of brain mri using knowledge-based multiple intermediator libraries. *Frontiers in Neuroscience*, 13:909, 2019.

[18] P. van Gelderen, J.A. de Zwart, and J.H. Duyn. Pittfalls of mri measurement of white matter perfusion based on arterial spin labeling. *Magnetic resonance in medicine*, 59:788–795, 4 2008.

[19] D. C. Alsop and J. A. Detre. Reduced transit-time sensitivity in noninvasive magnetic resonance imaging of human cerebral blood flow. *Journal of Cerebral Blood Flow Metabolism*, 16:1236–1249, 11 1996. doi: 10.1097/00004647-199611000-00019.

[20] M. A. Chappell, A. R. Groves, B. Whitcher, and M. W. Woolrich. Variational bayesian inference for a nonlinear forward model. *IEEE Transactions on Signal Processing*, 57:223–236, 2009.

[21] S. M. Smith. Fast robust automated brain extraction. *Human Brain Mapping*, 17:143–155, 11 2002. https://doi.org/10.1002/hbm.10062.

[22] Y. Zhang, M. Brady, and S. Smith. Segmentation of brain mr images through a hidden markov random field model and the expectation-maximization algorithm. *IEEE transactions on medical imaging*, 20:45–57, 1 2001.

[23] M. Craig. oxasl documentation release 0.0.1, 2021.

[24] J. C. Baron. Perfusion thresholds in human cerebral ischemia: historical perspective and therapeutic implications. *Cerebrovascular diseases (Basel, Switzerland)*, 11 Suppl 1:2–8, 2001.

[25] D. Crane, S. Black, A. Ganda, D. Mikulis, S. Nestor, and M. Donahue. Gray matter blood flow and volume are reduced in association with white matter hyperintensity lesion burden: a cross-sectional mri study, 2015.

[26] H. Okazawa, T. Tsujikawa, Y. Higashino, K. I. Kikuta, T. Mori, and A. Makino. No significant difference found in pet/mri cbf values reconstructed with ct-atlas-based and zte mr attenuation correction. *EJNMMI Research*, 9:26, 2019.

[27] H. Lu, C. Clingman, X. Golay, and P. C. M. van Zijl. Determining the longitudinal relaxation time (t1) of blood at 3.0 tesla. *Magnetic resonance in medicine*, 52:679–682, 9 2004.

[28] P. W. Hales, F. J. Kirkham, and C. A. Clark. A general model to calculate the spin-lattice (t1) relaxation time of blood, accounting for haematocrit, oxygen saturation and magnetic field strength. *Journal of cerebral blood flow and metabolism : official journal of the International Society of Cerebral Blood Flow and Metabolism*, 36:370–374, 2 2016.

[29] W. Li, P. Liu, H. Lu, J. J. Strouse, P. C. M. van Zijl, and Q. Qin. Fast measurement of blood t1 in the human carotid artery at 3t: Accuracy, precision, and reproducibility. *Magnetic Resonance in Medicine*, 77:2296–2302, 6 2017. https://doi.org/10.1002/mrm.26325.

[30] W. Dai, D. Garcia, C. de Bazelaire, and D. C. Alsop. Continuous flow-driven inversion for arterial spin labeling using pulsed radio frequency and gradient fields. *Magnetic Resonance in Medicine*, 60:1488–1497, 12 2008. https://doi.org/10.1002/mrm.21790.

[31] W. C. Wu, M. Fernández-Seara, J. A. Detre, F. W. Wehrli, and J. Wang. A theoretical and experimental investigation of the tagging efficiency of pseudocontinuous arterial spin labeling. *Magnetic resonance in medicine*, 58:1020–1027, 11 2007.

[32] W. D. Kovarik, T. S. Mayberg, A. M. Lam, T. L. Mathisen, and H. R. Winn. Succinylcholine does not change intracranial

pressure, cerebral blood flow velocity, or the electroencephalogram in patients with neurologic injury. *Anesthesia and analgesia*, 78:469–473, 3 1994.

[33] M.M. Brown, M.J. Parr, and A.R. Manara. The effect of suxamethonium on intracranial pressure and cerebral perfusion pressure in patients with severe head injuries following blunt trauma. *European journal of anaesthesiology*, 13:474–477, 9 1996.

[34] A.M. Renou, J. Vernhiet, P. Macrez, P. Constant, J. Billerey, and M. Y. Khadaroo. Cerebral blood flow and metabolism during etomidate anaesthesia in man. *British journal of anaesthesia*, 50:1047–1051, 10 1978.

[35] H. Takano, N. Motohashi, T. Uema, K. Ogawa, T. Ohnishi, and M. Nishikawa. Changes in regional cerebral blood flow during acute electroconvulsive therapy in patients with depression: positron emission tomographic study. *The British journal of psychiatry : the journal of mental science*, 190:63–68, 1 2007.

[36] T. Suwa, C. Namiki, S. Takaya, A. Oshita, K. Ishizu, and H. Fukuyama. Corticolimbic balance shift of regional glucose metabolism in depressed patients treated with ect. *Journal of Affective Disorders*, 136:1039–1046, 2012.

[37] M. Ota, T. Noda, N. Sato, K. Hattori, T. Teraishi, and H. Hori. Characteristic distributions of regional cerebral blood flow changes in major depressive disorder patients: a pseudo-continuous arterial spin labeling (pcasl) study. *Journal of affective disorders*, 165:59–63, 8 2014.

[38] N. Vasic, N. D. Wolf, G. Grön, Z. Sosic-Vasic, B. J. Connemann, and F. Sambataro. Baseline brain perfusion and brain structure in patients with major depression: a multimodal magnetic resonance imaging study. *Journal of psychiatry neuroscience : JPN*, 40:412–421, 11 2015.

[39] H. Järnum, S. F. Eskildsen, E. G. Steffensen, S. Lundbye-Christensen, C. W. Simonsen, and I. S. Thomsen. Longitudinal mri study of cortical thickness, perfusion, and metabolite levels in major depressive disorder. *Acta Psychiatrica Scandinavica*, 124:435–446, 12 2011. https://doi.org/10.1111/j.1600-0447.2011.01766.x.

[40] W. C. Drevets. Neuroimaging studies of mood disorders. *Biological Psychiatry*, 48:813–829, 2000.

[41] A.M. Leaver, M. Vasavada, S.H. Joshi, B. Wade, R.P. Woods, and R. Espinoza. Mechanisms of antidepressant response to electroconvulsive therapy studied with perfusion magnetic resonance imaging. *Biological Psychiatry*, 85:466–476, 2019.

[42] Z. Chen, X. Zhang, C. Yuan, X. Zhao, and M. J. P. van Osch. Measuring the labeling efficiency of pseudocontinuous arterial spin labeling. *Magnetic Resonance in Medicine*, 77:1841–1852, 5 2017. https://doi.org/10.1002/mrm.26266.

[43] J. B. Gonzalez-At, D. C. Alsop, and J. A. Detre. Cerebral perfusion and arterial transit time changes during task activation determined with continuous arterial spin labeling. *Magnetic Resonance in Medicine*, 43:739–746, 5 2000. https://doi.org/10.1002/(SICI)1522-2594(200005)43:5¡739::AID-MRM17¿3.0.CO;2-2.

[44] J. Kramme, J. Gregori, V. Diehl, V. I. Madai, F. C. von Samson-Himmelstjerna, and M. Lentschig. Improving perfusion quantification in arterial spin labeling for delayed arrival times by using optimized acquisition schemes. *Zeitschrift für Medizinische Physik*, 25:221–229, 2015.

[45] W. M. Teeuwisse, S. Schmid, E. Ghariq, I. M. Veer, and M. J. P. van Osch. Time-encoded pseudocontinuous arterial spin labeling: Basic properties and timing strategies for human applications. *Magnetic Resonance in Medicine*, 72:1712–1722, 12 2014. https://doi.org/10.1002/mrm.25083.

[46] W. M. Luh, S. L. Talagala, T. Q. Li, and P. A. Bandettini. Pseudo-continuous arterial spin labeling at 7 t for human brain: estimation and correction for off-resonance effects using a prescan. *Magnetic resonance in medicine*, 69:402–410, 2 2013.

2 Arterial spin labelling based global and regional postictal cerebral perfusion changes after ECT induced seizures

2.1 Introduction

Perfusion studies with ECT patients have been scarce. Moreover, to our knowledge, no postictal perfusion studies with ECT patients have been conducted up to now. Nuninga et al. [1] obtained ASL based rCBF in the hippocampi of 21 depressed patients one week before the start of ECT and one week after the tenth session. No significant differences were established. Leaver et al. [2] studied gCBF and rCBF in 57 patients with a major depressive episode. MRI scans were made 24 hours before the first ECT session, before the third session, after completing the course and six months thereafter. Again no significant changes were found in gCBF. However, in all patients rCBF was increased in the right anterior hippocampus after both two sessions and completing the ECT course. Neither of the above mentioned studies assessed postictal CBF. Postictal CBF may be the source of postictal behavioural impairments. The underlying hypothesis stems from animal research, suggesting that a vasoconstriction-induced hypoxia is a candidate mechanism for postictal hypoperfusion. Postictal perfusion studies in ECT patients have been hindered by practical feasibility issues, as hypoperfusion is time-sensitive [3] and can only be detected within one hour after the seizure. Measuring CBF within one hour will shine light on the possible occurrence of postictal hypoperfusion.
BL electrode placement is frequently associated with an increased amount of cognitive impairments [4, 5], compared to LUL or RUL electrode placement. The extent of postictal hypoperfusion seems to be associated with more cognitive impairments [3].
Adding to this, seizure duration may affect the extent of hypoxia in the postical phase. Like other postictal symptoms, postictal delirium may be related to postictal hypoperfusion. In one ECT study, seizure duration and postictal delirium were significantly correlated after adjusting for other covariates such as age, ECT parameters and diagnosis [6].
The electroencephalogram (EEG) has frequently been used to study the postictal state. A recent measure has been proposed in the evaluation of postictal EEG recovery, called the temporal brain symmetry index (tBSI) [7]. With this, a timely evolution of spectral characteristics can be determined. This may be the first quantitative measure to estimate postictal recovery time. The degree of EEG recovery may be correlated with the degree of postictal hypoperfusion measured with ASL. As discussed above postictal hypoperfusion may cease after one hour. Therefore, the moment of postictal ASL acquisition may affect the measured CBF. tBSI can be utilised to provide some context about brain recovery at the moment of ASL acquisition.
The aim of the current study is to assess the postictal gCBF and rCBF within one hour after an ECT session based on ASL, including the associations between postictal perfusion and seizure duration, electrode placement, time of postictal CBF measurement and EEG recovery, as well as some general patient characteristics. It is hypothesised that (1) CBF will be decreased in the first hour after an ECT induced seizure as compared with baseline, (2) seizure duration, electrode placement and the time to ASL (period of time between seizure initiation and ASL acquisition) will affect the calculated CBF and (3) the postictal level of EEG recovery will have a linear relation with the normalisation of postictal CBF values.

2.2 Methods

2.2.1 Study population and study design

For a description of the study population and study design, we refer to the subsection 'Study population and study design' in the general methods on page 9 of this thesis. Patients from the SYNAPSE with a baseline MRI scan and three postical MRI scans were included in the current study.

2.2.2 Image processing

Creating mean postictal CBF maps
Average postictal CBF maps were constructed to enable using the postictal MRI scans in the current study without unblinding, see Figure 4. The self-made CBF maps of all three MRI scans were merged, resulting

in a four-dimensional image consisting of three volumes. A mean CBF map was created by averaging those three volumes. In the mean CBF map each voxel represented the mean voxel value in the three maps. However, the three CBF maps based on the three postictal MRI scans were not identical. A certain voxel might be part of one of the CBF maps whereas the same voxel belongs to the background in other CBF maps of the same patient. The calculated mean of such voxels will be low because these voxels have no value in one or two CBF map(s). This results in voxels at the edge of the mean CBF map that have a low and unreliable value, as seen in Figure 4. By only including voxels that had a value above zero in all CBF maps, this problem was solved. To do so, first, all CBF maps were binarised. Those binarised CBF-masks were then merged and averaged. All voxels in the averaged CBF-mask had a value of 0.33, 0.66 or 1 representing a non-zero voxel value for that specific voxel in respectively one, two or three CBF maps. Only voxels that had a value of 1 were used in the final mask and multiplied with the original mean CBF map. In that way, the mean CBF map was created including only voxels present in all three CBF maps.

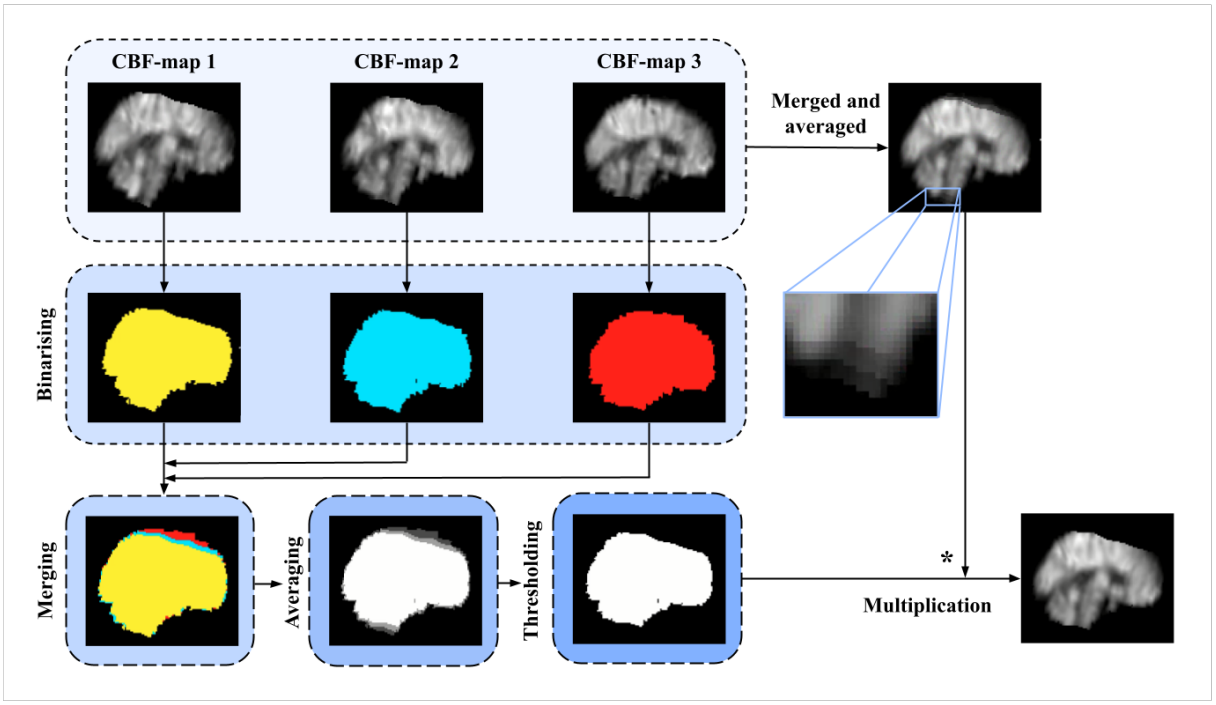

Figure 4: Step wise generation of a mean postictal CBF map. By binarising, merging, averaging and thresholding the three included CBF maps a mask is made representing only voxels that are present in all three CBF maps. Multiplying that mask with the initial merged and averaged CBF maps results in a mean postictal CBF map wherein all CBF maps contribute evenly.

Creating subtraction images

Baseline CBF maps were subtracted voxelwise from the postictal mean CBF maps to determine the change in perfusion. In correspondence with the three postictal scans, also the CBF maps of one patient made at different time points were not identical. Therefore, the CBF maps were binarised, merged, averaged and thresholded before subtraction in the same way as visualised in Figure 4. In that way, only voxels that had a value in both CBF maps were considered for analysis. A voxel in the subtraction images represented the absolute difference in CBF value for that particular voxel between baseline and the postictal phase. These absolute values were converted into percentages for a more robust analysis. A positive percentage indicates hyperperfusion and a negative percentage a hypoperfusion. Henceforward, when subtraction images are mentioned we refer to subtraction images with voxels representing the percentage change. These subtraction images were multiplied with the GM masks based on the corresponding baseline scan to only include GM. In some subtraction images, unreasonable high voxel values were found. Those values were not reliable and did presumably occur because of artefacts and small boundary values. The median ± three times the

standard deviation of the voxel values per patient and session were utilised to threshold the data and remove those outliers.
To visually assess the data, masks thresholded at different percentages of change were made. The subtracted images in this study were thresholded at values ranging from 10% to 35% perfusion change with intervals of 5%, see Figure 5.

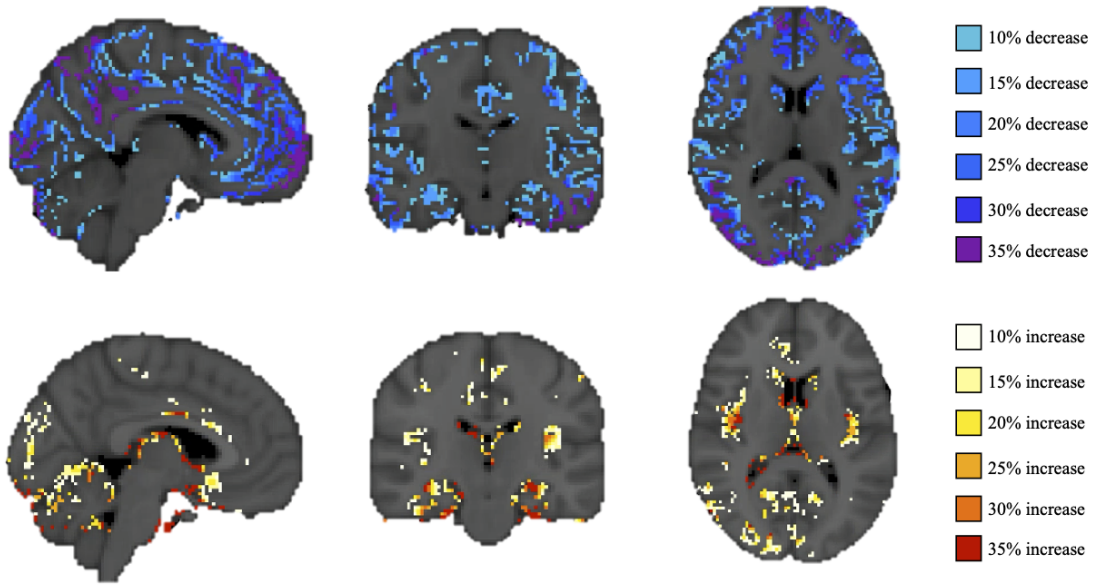

Figure 5: Thresholded subtraction images (postictal-baseline) of sub-008 (upper) and sub-004 (lower). The upper panel shows the percentage decrease in the perfusion per voxel and the lower panel shows the percentage increase per voxel. F.l.t.r sagittal, coronal and transverse plane.

2.2.3 Global descriptive analysis

A global descriptive analysis was done based on the subtraction images to get an impression of the (variability in the) data. The degree of change in perfusion between the baseline and mean postictal scan was categorised. Five categories were defined based on the following requirements. In those requirements, regions refer to the four lobes and cerebellum and a cluster of nine adjacent voxels had to have a three-by-three formation.

None	1. Random distributed spots of perfusion change with different percentages. 2. Only one or two voxels thick boundaries of perfusion change visible. 3. No clusters in the two dimensional images where the perfusion change is consistent over a cluster of nine adjacent voxels. Whereby consistent is defined as at most 10% difference between the nine adjacent voxels.
Mild	1. Random distributed spots of perfusion change with different percentages forming at least three clusters of nine adjacent voxels. 2. Perfusion changes of at least 20% seen in two or more regions, in nine adjacent voxels.
Moderate	1. More than half of the cerebral GM voxels show a perfusion change. 2. Perfusion changes of at least 20% seen in two or more regions, in nine adjacent voxels.
Severe	1. More than 80% of the cerebral GM voxels show a perfusion change. 2. More than 50% of all change in perfusion is at least 20% per voxel. 3. Perfusion changes of at least 20% are seen in three or more regions, in nine adjacent voxels.
Very severe	1. More than 50% of all change in perfusion is at least 35% per voxel. 2. Changes in perfusion of at least 20% are seen in all regions, in nine adjacent voxels.

2.2.4 Regional CBF

Regions

The regional analyses were performed in the four lobes of the cortex and the cerebellum. These regions were localised within standard space with the MNI Structural Atlas in FSLeyes [8] part of FSL. The MNI Structural Atlas consisted of probability maps; every voxel had a value between 0 and 100 indicating the probability that the voxel belonged to a certain region. To binarise these maps, they were thresholded at 25% probability to ensure minimal overlap between different regions and enough room for variability in the data, see Figure 6.

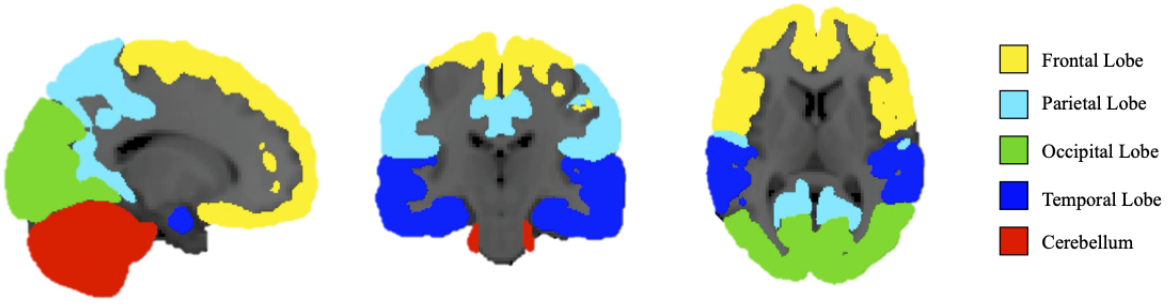

Figure 6: Spatial maps for the frontal, parietal, occipital and temporal lobe and the cerebellum in standard space. F.l.t.r sagittal, coronal and transverse plane.

The mean percentage change per region was calculated by multiplying the binary region mask with the GM masked subtraction images. However, some pre-processing was necessitated. A morphological operation within FSL was performed to sub-sample the isotropic voxels of the atlas-based regions to the voxel size of the CBF maps. Moreover, some voxels within the GM region of subtraction images had a value of zero. Those value are important for the mean calculation because they represent the voxels in the GM that did not change between baseline and postictal. Including those voxels was done by multiplying the mean of the non zero voxels by the number of non-zero voxels and divide the outcome by the number of all voxels in the region.
In some regions both increases and decreases in perfusion occurred. When the mean perfusion change was calculated, large changes in a small part of a region can cancel out. Therefore, next to the total perfusion change, also a perfusion increase and decrease were calculated. Whereby only the voxels representing respectively an increase or decrease in perfusion were taken into account. Moreover, the number of GM voxels within a specific region was calculated. To ensure robust analysis, regions smaller than 50 voxels were excluded from the analysis.

Regional descriptive analysis

Because of large variability and a lack of power, regional results will be presented in a descriptive way, without statistical analyses. A regional descriptive analysis was developed and carried out to find changes in perfusion in specific regions. The subtraction images that represented complete change in perfusion were utilised for this analysis. In other words, increases and decreases in perfusion per voxel were not assessed separately. Farrell et al. [3] defined hypoperfusion as a decrease in CBF of at least 10 ml/100g/min compared to baseline. They also defined a normal gCBF to be 60 ml/100g/min. So, they considered a perfusion decrease of approximately 16.7% to be hypoperfusion. The calculation of this percentage is an interpretation of the choices made by Farrell et al. [3], and not a hard threshold. To account for the uncertainty in this percentage its value was rounded to two significant digits. In the current study, hypoperfusion and hyperperfusion were defined as a decrease and increase of 17% in perfusion, respectively. Regional hypoperfusion is therefore defined according to the following three criteria: (1) at least half of all patients show a decrease in perfusion of at least 17%, (2) on top of that, at least two-thirds of all patients show a decrease in perfusion and (3) within the tolerated one-third of patients that do not show a decrease in perfusion at most two show an increase larger than 17%. Vice versa, those criteria also apply for hyperperfusion.

2.2.5 Postictal EEG recovery

Postictal EEG recovery can be quantified with the temporal brain symmetry index (tBSI) which is an extension of the original BSI [9]. Hereby, the normalised difference between the considered spectral characteristics and a baseline EEG epoch is calculated. See Equation 1, with $S_{i,j}$ the Fourier coefficient belonging to frequency $i = 1, ..., N$ of bipolar derivations $j = 1, 2, ..., K$ [9].

$$tBSI' = \frac{1}{N}\sum_{i=1}^{N}\frac{1}{K}\sum_{j=1}^{K}\left\|\frac{S_{i,j}-S_{ref,i,j}}{S_{i,j}+S_{ref,i,j}}\right\| \tag{1}$$

EEGs were bandpass filtered between 1 and 25 Hz with a first-order Butterworth filter. The normalised difference between postictal and baseline spectral characteristics was determined per five-second epoch utilising Welch's averaged periodogram method. Values ranged between zero and one. A value of zero indicated maximal asymmetry and a value of one perfect symmetry between the baseline and postictal epoch. A time constant (τ) was calculated based on fitting an exponential function to the tBSI data, see Equation 2. Coefficients $a0$ and a were estimated. Complete explanation of the estimation of the coefficients goes beyond the scope of this thesis.

$$a0 - a * e^{-\frac{t}{\tau}} \tag{2}$$

Resulting coefficients were used for extrapolation to the moment of CBF measurement with pCASL.
At seizure offset the EEG is characterised by so-called postictal suppression [10]. After some time, the EEG will recover to its baseline activity. The goal of SYNAPSE is to visualise postictal hypoperfusion within one hour after seizure initiation. The EEG and recovery thereof can provide information about hypoperfusion as well [11]. The extend of EEG recovery at the moment of CBF measurement is of interest because it may reflect the extend of postictal hypoperfusion found with pCASL. Because the EEG recording is terminated before the start of ASL acquisition, the tBSI is extrapolated to that moment based on the slope of the EEG recovery curve.

2.2.6 Statistical analysis

To assess (1) the possible differences in CBF measured at baseline and one hour after an ECT induced seizure and (2) to find possible effects of seizure duration, electrode placement, time to ASL , and level of EEG-recovery on that correlation, multiple statistical tests were performed. Missing data were prevalent and patients were measured repeatedly, introducing a nested structure in the data. A linear mixed-effects model works well with low sample sizes, accounts for structured data and allows using all data even though some data points are missing. Therefore, a linear mixed-effects model was used in the current study. There are multiple types of linear mixed-effects models. A random intercept model assumes that patients have separate baseline values (i.e. random intercept). Next to that, it expects that all patients respond in the same way to the explanatory variable. A random coefficients model (i.e. random intercept and random slope) allows each group, in this case: each patient, to have a different slope and thus react differently on the explanatory variable. The first model (1) was a random intercepts model and the second model (2) a random coefficients model.
In the models, gCBF was the dependent variable because we are interested in how several parameters impact the measured gCBF. In a linear mixed-effects model, a distinction is made between fixed effects and random effects. Variables that are suspected to influence the dependent variable, and are measured at specific instances of interest are considered fixed effects. For the first part of the statistical analysis (1), the fixed effect was the session, because a difference was expected between the gCBF measured at baseline and post-seizure. The fixed effects for (2) were the seizure duration, electrode placement, time to ASL and level of EEG recovery. Random effects are usually grouping factors measured at randomly chosen instances only as representatives of the study population and might influence the patterns we see. In both models, the patients were the random effects. A two-tailed p-value of <0.05 was considered statistically significant. R (R Core Team, version 1.4.1717, Vienna, Austria [12]) was used for statistical analysis.

2.3 Results

A total of eleven patients were included from the twenty patients included in the SYNAPSE at the start of data analysis. Data of two patients were not available yet, four patients dropped out of the SYNAPSE and five patients did not undergo MRI or stopped with MRI after baseline. An overview of patient characteristics is given in Table 2. The mean age was 47.5 ± 12.8 years, 55% was female and 64% was treated with BL electrode placement. Mean postictal CBF maps were made and analysed, therefore the mean seizure duration, mean time to ASL and mean tBSI are given in Table 2.

Table 2: Patient characteristics

Patient	Sex	Age (yrs)	Electrode placement	Mean seizure duration ± SD (s)	Mean time to ASL ± SD (min)	Mean tBSI ± SD (s)
sub-001	m	42	BL	60.7 ± 2.7	63.13 ± 6.22	0.77 ± 0.06
sub-003	f	44	RUL	65.1 ± 4.1	64.61 ± 10.73	0.74 ± 0.06
sub-004	f	24	BL	92.6 ± 27.1	64.63 ± 12.36	0.62 ± 0.08
sub-006	f	45	BL	52.4 ± 4.4	56.13 ± 2.52	0.64 ± 0.08
sub-007	m	43	BL	55.1 ± 5.5	69.33 ± 7.57	0.80 ± 0.04
sub-008	f	47	BL	69.6 ± 19.9	65.33 ± 14.29	0.67 ± 0.13
sub-009	m	45	RUL	87.9 ± 22.9	66.33 ± 14.36	0.65 ± 0.02
sub-011	m	74	BL	44.6 ± 4.9	74.67 ± 13.61	0.66 ± 0.05
sub-012	m	42	LUL	46.5 ± 9.3	61.67 ± 10.26	0.69 ± 0.05
sub-013	f	55	RUL	46.7 ± 1.6	63.53 ± 5.22	0.75 ± 0.02
sub-018	f	62	BL	33.9 ± 8.8	66.18 ± 15.55	0.79 ± 0.03

m = male; f = female; ; BL = bifrontotemporal; RUL = right unilateral; LUL = left unilateral; SD = standard deviation; BSI = brain symmetry index

2.3.1 Global CBF values

The gCBF values based on the self-made CBF maps are seen in Table 7. The results of the CBF data were variable with differences within and between subjects (mean=42.36 ± 13.99, min=12.91, max=65.29 ml/100g/min).
In Figure 7, the gCBF values per patient are given for both the baseline MRI scan and the mean of the three postictal MRI scans. The absolute gCBF values differ per patient. Seven out of eleven patients showed a postictal decrease in perfusion compared to baseline.

Table 3: gCBF values per patient, at baseline and after three separate ECT sessions, in ml/100g/min based on the self-made CBF maps. Values below 20 ml/100g/min are coloured in red because they indicate severe hypoperfusion.

	Baseline	Postictal *t=1*	Postictal *t=2*	Postictal *t=3*
sub-001	40.45	43.96	32.94	38.09
sub-003	30.70	45.66	41.18	37.57
sub-004	63.30	62.6	57.08	65.29
sub-006	41.29	31.49	35.06	27.04
sub-007	38.83	46.74	43.79	37.88
sub-008	62.38	50.78	45.82	61.69
sub-009	45.27	19.00	24.05	23.47
sub-011	18.63	12.91	23.05	13.51
sub-012	48.30	51.65	56.12	45.38
sub-013	46.02	54.70	59.53	51.92
sub-018	52.55	52.40	52.06	51.96

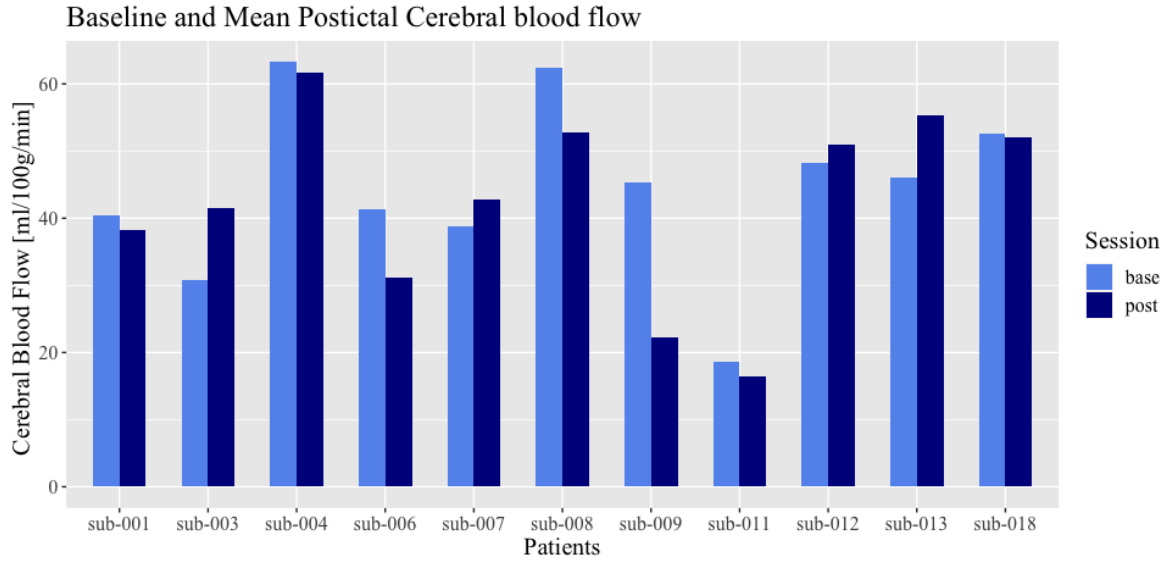

Figure 7: Absolute gCBF values per patient whereby light blue indicates the baseline (base) gCBF values and dark blue the postical (post) values.

Two linear mixed-effect models were utilised to answer questions (1) and (2) as stated in the methods. The results of the first model are presented under the first blue row in Table 4. Baseline and mean postictal gCBF values were included in the first model. The estimate of the dependent variable (gCBF) was 74.572 ml/100g/min whereby the averaged postictal gCBF values were 1.772 ml/100g/min lower after correction for age and sex. Both age and sex have a nearly significant effect on the gCBF values ($p = 0.051$ and $p = 0.057$, respectively). In the second model, one patient was excluded because it was the only patient treated with LUL electrode placement. Creating a separate group in the model based on just one patient was considered unreliable, leaving ten patients for analysis. The outcomes of the second model are presented under the second blue row in Table 4. All postictal gCBF values were included without averaging. After correction for all other included fixed effects, a statistically significant effect of seizure duration was seen on the postictal gCBF ($p = 0.041$). Indicating that a longer seizure duration may result in more postictal hypoperfusion. Based on visual assessment of the Q-Q-plot, the residuals were normally and not perfectly normally distributed in the first and second model, respectively.

Table 4: Results of the two linear mixed-effects models.

	Estimate	*SE*	df	*t*	*p*
Baseline and mean postictal scans					
Intercept gCBF	74.572	11.661	9.351	6.395	1.064e-4 ***
Age	-0.520	0.235	9.000	-2.256	0.051 .
Sex male	-12.533	5.737	8.995	-2.185	0.057 .
Session postictal	-1.772	2.863	10.409	-0.619	0.549
Postictal scans					
Intercept gCBF	95.123	20.418	15.332	4.610	3.221e-4 ***
Age	-0.535	0.316	6.505	-1.698	0.137
Sex male	-16.295	7.940	5.933	-2.052	0.086 .
Electrode placement unilateral	-2.40	8.299	5.843	-0.354	0.736
Seizure duration	-0.170	0.077	16.449	-2.218	0.041 *
Time to ASL	0.029	0.094	16.029	0.306	0.763
Level of EEG recovery	-16.145	15.638	17.580	-1.032	0.316

SE= standard error, df = degrees of freedom, significance codes: 0 '***' 0.05 '.'

2.3.2 Global descriptive analysis

Based on the proposed criteria, subtraction images of all patients with three postictal MRI scans were divided into five categories, see Table 5. Subtraction images including solely voxels representing an increase or decrease in perfusion were assessed separately to understand the generation of the difference in postictal gCBF values compared to baseline. A perfusion change is considered from the category 'mild' and upward based on the subtraction image. Five patients show both an increase and decrease in perfusion. Two patients show only an increase and four patients only a decrease. Based on the descriptive analysis, three patients are considered to show postictal hypoperfusion because the subtraction scan representing the decrease in perfusion of those patients falls within a higher category compared with the subtraction scan representing the increase in perfusion. Whereas according to the absolute gCBF values, see Figure 7, seven patients show a decrease in postictal perfusion compared to baseline. The subtraction images of sub-003, sub-007, sub-013 and sub-018 are classified by the descriptive analysis as showing an increase in perfusion. Whereas the absolute gCBF values in Figure 7, show an increase in postictal perfusion in sub-003, sub-007, sub-012 and sub-013. Thus, there is some discrepancy between the categorical descriptive analysis and the absolute values.

Table 5: Categorisation of the thresholded subtraction images.

Patient	Increase in perfusion	Decrease in perfusion
sub-001	None	Moderate
sub-003	Severe	None
sub-004	Mild	Mild
sub-006	Mild	Mild
sub-007	Mild	None
sub-008	Mild	Moderate
sub-009	None	Very severe
sub-011	Mild	Mild
sub-012	Mild	Mild
sub-013	Moderate	None
sub-018	Mild	None

2.3.3 Regional descriptive analysis

According to the criteria for regional hypoperfusion and hyperperfusion in the four lobes and the cerebellum, no regional hypoperfusion was found in the subtraction images, see Table 6. Among patients, the changes per region varied considerably (columns). The perfusion changes between regions within the same patient are more consistent (rows).

Table 6: Regional percentage difference between baseline and postictal subtraction images.

Patient	Frontal lobe	Parietal lobe	Occipital lobe	Temporal lobe	Cerebellum
sub-001	-24.03	-24.01	-21.81	-17.23	-5.57
sub-003	28.41	30. 87	34.08	47.20	41.50
sub-004	-7.97	-4.24	10.03	6.25	19. 61
sub-006	-11.32	-7.78	5.76	-9.62	-0.27
sub-007	12.85	12.54	10.62	5.56	0.10
sub-008	-20.82	-21.98	-20.60	-13.86	-13.75
sub-009	-48.94	-49.11	-27.51	-37.84	-17.53
sub-011	-8.46	6.94	66.55	13.66	33.30
sub-012	1.20	-0.83	-2.11	3.48	1.53
sub-013	20.54	19.13	24.13	18.18	12.62
sub-018	0.87	0.13	-4.46	-0.63	0.34

Colour-code: green = hypoperfusion (more than 17% decrease), light green = decrease in perfusion smaller than 17%, red = hyperperfusion (more than 17% increase), pink = increase in perfusion smaller than 17%.

2.4 Discussion

The short-term effect of ECT induced seizures on cerebral perfusion was assessed with pCASL MRI. Seven out of eleven patients showed a postictal decrease in perfusion compared to baseline. The proposed method for a descriptive analysis of the changes in gCBF was not accurate enough to differentiate between all changes involved in the baseline and postical CBF maps. Also, neither hypoperfusion nor hyperperfusion were found in the four lobes and cerebellum according to the proposed regional descriptive analysis of CBF. Based on a linear mixed-effects model postictal gCBF was not significantly different compared to baseline. Nevertheless, a significant negative correlation was found between seizure duration and postictal gCBF.

Descriptive analyses
A lack of power in the current data set led to the conception of global and regional descriptive analyses. The global descriptive analysis based on the classification of subtraction images into five categories was not accurate enough to distinguish between the small differences between baseline and postictal CBF values in patients. A reason for this could be the large variability in the absolute CBF values. The descriptive analysis might benefit from the definition of an extra category between mild and moderate. The regional descriptive analysis including the four lobes and cerebellum was based on differences in perfusion of at least 17%. None of the regions could be classified as showing hypo- or hyperperfusion based on this analysis. Based on Table 6, this conclusion may be solid because large inter-patient and small intra-patient variability in rCBF changes were seen. By including smaller regions the proposed regional analysis can be improved.
Currently, no large disparity was found between the several regions within patients. The effect of changes in smaller regions might be currently cancelled out by examining large areas of the brain, resulting in approximately the same rCBF values in all regions. This theory is supported by literature, where changes in CBF are often reported in small regions of the brain [13–15]. Also, Farrell et al. [3] concluded that postictal hypoperfusion in epilepsy patients is a local phenomenon after locating the hypoperfusion specifically in regions involved in the seizure. In future research, brain structures subjected to seizure activity, such as cortical regions underneath the ECT-electrodes, should be included in the regional analysis. Also, the design of the descriptive analyses might be improved by organising a consensus meeting with experts in the field.

Postictal CBF compared to baseline
In the current study, no significant differences were found between baseline and postictal gCBF. With a study design similar to the current Farrell et al. [3] utilised pCASL MRI to determine CBF within one hour of a habitual seizure in ten patients with focal epilepsy. Maximal postictal gCBF reductions of at least 10 ml/100g/min were found in eight out of ten patients. In th same study quantitative CBF data was obtained based on manually drawn ROIs in single brain areas exhibiting the maximal postictal CBF decreases. In those ROIs, all adjacent voxels with a CBF change of at least 10 ml/100g/min were included. A mean reduction of 26.6 ± 6.0% in CBF compared to baseline was found in those ROIs. Although both methods suggest postictal hypoperfusion no statistically significant differences were found.
Takano et al. [15] assessed gCBF before, during and after ECT induced seizures with $^{15}O - H_2O$-PET in six depressed patients. After a significant interictal increase in gCBF, values returned to baseline 10-30 minutes post-seizure. Another study, including six epilepsy patients and perfusion weighted imaging, reported the same finding of initial reduction in CBF followed by a normalisation towards baseline [16]. The bolus-peak-ratio was determined as a semiquantitative measure of CBF and rose back to baseline values 28-72 minutes post-seizure. These studies [15, 16] suggest that postictal hypoperfusion lasts about half an hour. Nevertheless, the study populations are small and heterogeneous. Moreover, Scott et al. [17] found a significant rCBF reduction in the inferior anterior cingulate cortex 45 minutes after an ECT induced seizure with SPECT in depressed patients. Next to that, gCBF reductions of at least 15 ml/100g/min were found in twelve out of thirteen people within 80 minutes after seizure utilising computed tomography perfusion measurements [18].
Thus, postictal reduction in gCBF and rCBF have been replicated but results are not always statistically significant [3, 18], as is the case in the current study. The inconsistency in literature suggests a relation between postictal perfusion and moment of CBF measurement and the ROI.

Factors affecting postictal CBF
Whereas age, sex, electrode placement, time to ASL and level of EEG recovery did not have a significant effect on the postictal gCBF, seizure duration showed a significant negative correlation. A finding supported by previous studies [3, 18]. This suggests that prolonged seizure activity and thus prolonged general neuronal firing is more demanding on the brain and results in more severe hypoperfusion.
The variable 'time to ASL' represents the period of time between seizure initiation and the start of pCASL MRI acquisition. Factually, this is the time point in the postictal state at which the CBF is measured. Although this factor was not significantly correlated with postictal gCBF in the current study, several authors described the relevance of this parameter on the determined CBF [3, 16, 18, 19]. The discrepancy in studies assessing the postictal perfusion, may be based on the moment of measurement. Based on observations of severe hypoxia in rats, postictal hypoperfusion is preferably measured 20-60 minutes post-seizure [3]. Therefore, we aimed to measured CBF within one hour after the ECT stimulus. However, the start of ASL acquisition frequently exceeded this time frame due to patient safety issues (e.g., recurrence of consciousness before leaving the recovery room after anaesthesia) and logistics (e.g. availability of the MRI scan). This might explain why the time to ASL was not significantly correlated with the postictal CBF.

Strengths and limitations
Evaluating the current study several strengths can be specified. Firstly, all included patients underwent both the baseline and all three postictal scans thus there was no missing data. Moreover, this study included patients, which were severely ill, to examine potential new insight in the postictal phase.
This study also had several shortcomings. First of all, preliminary data from the blinded SYNAPSE was utilised which resulted in three postictal scans possibly affected by the unknown intervention. Within SYNAPSE, it is sought to reduce postictal hypoperfusion with vasodilatory drugs. Two of the three postictal scans involved a pre-ECT administration of vasodilatory drugs that may have influenced postictal CBF. Although mean postictal CBF maps were utilised in the current study, these maps are polluted with the unknown effect of the interventions probably interacting with the measured postical CBF. Secondly, circumstances under which the baseline and postical scans were made varied. At baseline, patients might have drunk coffee or smoked before the ASL acquisition. Whereas before the postictal scan patients underwent an ECT session engendering a variety of parameters that interfere with CBF. Such as preoxygenation before the ECT-stimulus and administration of etomidate [20–22] and benzodiazepines or propofol [15], in case of severe postictal confusion. As discussed, late and variable timing of postictal CBF measurement was another limitation. Next to that, multiple studies determined the seizure onset zone per patient and found local hypoperfusion especially in those areas of the brain [3, 18]. In the current study, the seizure onset zone was not defined which made it more difficult to locate small changes in perfusion. The current study is preliminary and should be interpreted as such. Only eleven patients were included in the current preliminary study limiting the sample size. Lastly, the current study is preliminary and should be interpreted as such. The residuals of the utilised mixed-effects model were not strictly normally distributed. Therefore, the results of the model may not be accurate and prone to overinterpretation.

Clinical relevance
Postictal symptoms form a considerable burden in the continuation and use of ECT in depressed patients. To understand the cause of these symptoms we need to learn more about the aftermath of seizures. Measuring the postictal perfusion is part of this process. In the current study, a negative correlation was suggested between seizure duration and postictal CBF. Thus, a longer seizure duration might result in more severe postictal hypoperfusion and postictal symptoms. Potentially, vasodilatory drugs can be administered after long ECT induced seizures to facilitate postictal recovery of the brain and reduce postictal symptoms.

Conclusion
In conclusion, no statistically significant postictal cerebral hypoperfusion was found. A significant correlation was found between longer seizure duration and lower postictal gCBF. No correlations were found between the postictal gCBF and electrode placement, time to ASL and level of EEG recovery. Future research should focus on local changes in perfusion preferably in the seizure onset zone, within one hour post-seizure.

References

[1] J.O. Nuninga, R.C.W. Mandl, M. Froeling, J. C.W. Siero, M. Somers, M.P. Boks, and W. Nieuwdorp. Vasogenic edema versus neuroplasticity as neural correlates of hippocampal volume increase following electroconvulsive therapy. *Brain stimulation*, 13:1080–1086, 2020.

[2] A.M. Leaver, M. Vasavada, S.H. Joshi, B. Wade, R.P. Woods, and R. Espinoza. Mechanisms of antidepressant response to electroconvulsive therapy studied with perfusion magnetic resonance imaging. *Biological Psychiatry*, 85:466–476, 2019.

[3] J. S. Farrell, I. Gaxiola-Valdez, M. D. Wolff, L. S. David, H. I. Dika, and B. L. Geeraert. Postictal behavioural impairments are due to a severe prolonged hypoperfusion/hypoxia event that is cox-2 dependent. *eLife*, 5:e19352, 11 2016.

[4] W. H. Lee, Z. D. Deng, T. S. Kim, A. F. Laine, S. H. Lisanby, and A. V. Peterchev. Regional electric field induced by electroconvulsive therapy in a realistic finite element head model: Influence of white matter anisotropic conductivity. *NeuroImage*, 59:2110–2123, 2012.

[5] D. M. Martin, V. Gálvez, and C. K. Loo. Predicting retrograde autobiographical memory changes following electroconvulsive therapy: Relationships between individual, treatment, and early clinical factors. *The international journal of neuropsychopharmacology*, 18, 6 2015.

[6] I. M. Reti, A. Krishnan, A. Podlisky, A. Sharp, and W. Melinda. Predictors of electroconvulsive therapy postictal delirium. *Psychosomatics*, 55:272–279, 2014.

[7] M. J. A. M. van Putten, J. M. Peters, S. M. Mulder, J. A. M. de Haas, C. M.A. Bruijninckx, and D. L. J. Tavy. A brain symmetry index (bsi) for online eeg monitoring in carotid endarterectomy. *Clinical Neurophysiology*, 115:1189–1194, 2004.

[8] P. McCarthy. Fsleyes, 2021.

[9] M. J. A. M. van Putten. Extended bsi for continuous eeg monitoring in carotid endarterectomy. *Clinical Neurophysiology*, 117:2661–2666, 12 2006.

[10] Julia C M Pottkämper, Joey P A J Verdijk, Jeannette Hofmeijer, Jeroen A van Waarde, and Michel J A M van Putten. Seizures induced in electroconvulsive therapy as a human epilepsy model: A comparative case study. *Epilepsia Open*, n/a, 8 2021. https://doi.org/10.1002/epi4.12532.

[11] B. Razavi and K. Meador. Dynamics of quantitative eeg changes during cerebral hypoperfusion (p4.075). *Neurology*, 86:P4.075, 4 2016.

[12] R Core Team. R: A language and environment for statistical computing., 2021.

[13] T. C. Ho, J. Wu, D. D. Shin, T. T. Liu, S. F. Tapert, and G. Yang. Altered cerebral perfusion in executive, affective, and motor networks during adolescent depression. *Journal of the American Academy of Child Adolescent Psychiatry*, 52:1076–1091.e2, 2013.

[14] M. Ota, T. Noda, N. Sato, K. Hattori, T. Teraishi, and H. Hori. Characteristic distributions of regional cerebral blood flow changes in major depressive disorder patients: a pseudo-continuous arterial spin labeling (pcasl) study. *Journal of affective disorders*, 165:59–63, 8 2014.

[15] H. Takano, N. Motohashi, T. Uema, K. Ogawa, T. Ohnishi, and M. Nishikawa. Changes in regional cerebral blood flow during acute electroconvulsive therapy in patients with depression: positron emission tomographic study. *The British journal of psychiatry : the journal of mental science*, 190:63–68, 1 2007.

[16] G. Leonhardt, A. De Greiff, J. Weber, T. Ludwig, H. Wiedemayer, and M. Forsting. Brain perfusion following single seizures. *Epilepsia*, 46:1943–1949, 12 2005. doi: 10.1111/j.1528-1167.2005.00336.x.

[17] A. I. F. Scott, N. Dougall, M. Ross, R. E. O'Carroll, W. Riddle, and K. P. Ebmeier. Short-term effects of electroconvulsive treatment on the uptake of99mtc-exametazime into brain in major depression shown with single photon emission tomography. *Journal of Affective Disorders*, 30:27–34, 1994.

[18] E. Li, C. D. d'Esterre, I. Gaxiola-Valdez, T. Y. Lee, B. Menon, and J. S. Peedicail. Ct perfusion measurement of postictal hypoperfusion: localization of the seizure onset zone and patterns of spread. *Neuroradiology*, 61:991–1010, 2019.

[19] T. J. Milo, G. E. Kaufman, W. E. Barnes, L. M. Konopka, J. W. Crayton, and J. G. Ringelstein. Changes in regional cerebral blood flow after electroconvulsive therapy for depression. *The Journal of ECT*, 17, 2001.

[20] A.M. Renou, J. Vernhiet, P. Macrez, P. Constant, J. Billerey, and M. Y. Khadaroo. Cerebral blood flow and metabolism during etomidate anaesthesia in man. *British journal of anaesthesia*, 50:1047–1051, 10 1978.

[21] L.N. Milde, J.H. Milde, and J.D. Michenfelder. Cerebral functional, metabolic, and hemodynamic effects of etomidate in dogs. *Anesthesiology*, 63:371–377, 10 1985.

[22] S.C. Robertson, P. Brown, and C.M. Loftus. Effects of etomidate administration on cerebral collateral flow. *Neurosurgery*, 43:314–317, 8 1998.

3 In search of antidepressant ECT mechanisms: relation between clinical effect and perfusion changes in candidate brain regions

3.1 Introduction

The response rate of ECT varies between 50% and 80% depending on the subtype of MDD and the effectiveness of prior pharmacotherapy trials [1–3]. Although its effectiveness in the majority of MDD patients, ECT is mostly indicated for treatment-resistant patients in The Netherlands [4]. As a consequence, ECT is often the last option for remission of MDD patients that already underwent at least two consecutive trials of ineffective psychopharmacological treatments. It is still unclear why ECT is ineffective in some patients, partly because the specific antidepressant working mechanisms of ECT remain unknown [5].
Numerous studies assessed the neural effects of ECT on the human brain. Although the ECT induced seizures are referred to as generalised, not all brain networks and regions are equally involved [6, 7]. Most neuroimaging studies addressing the effects of ECT, found several involved brain regions instead of whole-brain effects [8–14]. However, how regional changes contribute to the efficacy of ECT is less clear [14–18]. Differentiation between nonspecific effects and effects associated with, and possibly responsible for, antidepressant response to ECT, remains a topic of interest.
Antidepressant effects of ECT are expected in regions that are altered in MDD. However, MDD is a heterogeneous disease and as a result, there is no consensus about the specific brain regions or structures involved [19]. Nonetheless, various neuroimaging studies were conducted to determine regions of altered rCBF in patients with MDD. In most studies, SPECT, PET or ASL MRI was utilised. In MDD patients, a decrease in rCBF is often replicated in the prefrontal cortex [20–25], anterior cingulate cortex [20, 21, 23, 24, 26, 27], parahippocampal cortex [21, 26, 28] and frontal lobe [27, 29, 30]. An increase in rCBF was found in the amygdala [23, 31–33]. These regions with altered rCBF may serve as key elements in the substantiation of ECT efficacy and will be analysed in the current study by utilising pCASL MRI. Next to that, the hippocampus will be included, because of its known role in MDD and observed functional changes after ECT [34–37].
The aim of the current preliminary study is to relate altered gCBF and rCBF measured with pCASL in predefined brain regions to the antidepressant effect of ECT. It is hypothesised that clinical remission of the depression is associated with an improvement in rCBF in the regions known to show altered rCBF in patients with MDD.

3.2 Methods

3.2.1 Study population and study design

For a description of the study population and study design, we refer to the subsection 'Study population and study design' in the general methods on page 9 of this thesis. In the current study, MRI scans made at baseline, end-ECT and follow-up were utilised.

3.2.2 Quantification of ECT response

The effectiveness of ECT was assessed with the 17-item Hamilton Rating Scale for Depression (HRSD). A post-treatment decrease in HRSD-score of at least 50% compared to baseline was defined as treatment response [38, 39]. The HRSD was scored at baseline, at most two weeks after termination of the ECT course (end-ECT) and three months thereafter (follow-up). For the analysis, the study population was divided into non-responders and responders based on the HRSD-score at end-ECT.

3.2.3 Determining regions affected in MDD

Based on earlier research, six regions that showed significant altered CBF in MDD patients compared to healthy controls were considered in the current regional analysis. The included subcortical and cortical structures were the hippocampus, amygdala, prefrontal cortex, also called frontal pole, cingulate cortex, parahippocampal cortex and frontal lobe. Besides the binary Oxford-Imanova Striatal Structural Atlas, both the Harvard-Oxford Subcortical and Cortical Structures Atlas were used to make masks for these regions. Only the latter two, had to be thresholded at 50% to make a binary mask. All included regions are visualised in Figure 8. Region masks were utilised to find the GM voxels in the self-made CBF maps or subtraction images that were part of a specific region. The amount of GM voxels included per region was calculated per patient. A minimum of 35 GM voxels per region was required to be included in the analysis.

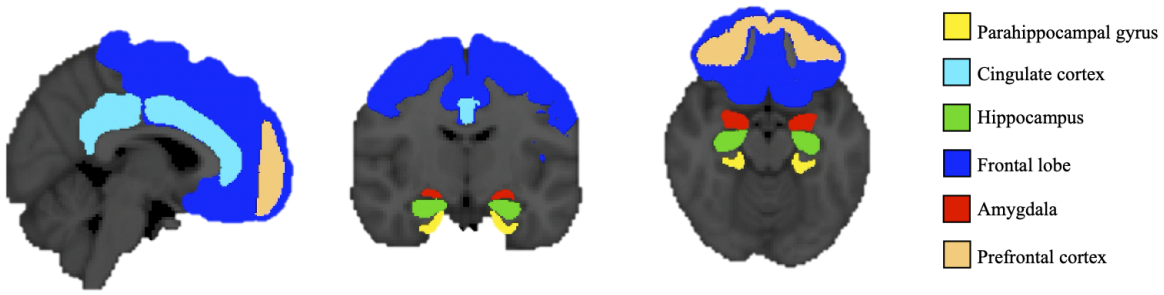

Figure 8: Brain regions included in the current study visualised in f.l.t.r sagittal, coronal and transverse plane.

3.2.4 Statistical analysis

Two linear mixed-effects models were utilised to assess the association between improvement in HRSD-score over the course of ECT and 1) changes in the gCBF and 2) changes in rCBF of predefined regions. Both models were random intercepts models. These models were a good fit for the current data because of the repeated measures, low sample sizes and missing data points. The CBF values and HRSD-scores were normalised by dividing the respective parameters by their corresponding baseline value. This was considered more robust because the absolute values of both CBF and HRSD-score varied considerably between patients. In the first model, normalised HRSD-score was the dependent variable. Normalised gCBF values, age and sex were fixed effects and patients the random effect. In the second model, rCBF values of all regions mentioned above were included as fixed effects instead of the gCBF. A two-tailed p-value of <0.05 was considered statistically significant. R (R Core Team, version 1.4.1717, Vienna, Austria [40]) was used for statistical analysis.

3.3 Results

In total, twelve patients were included. Twelve baseline, eleven end-ECT and eight follow-up MRI scans were available for analyses. The gCBF values at baseline, end-ECT and follow-up are given in Table 7, values below 20 ml/100g/min are coloured in red because they indicate severe hypoperfusion. In the next three rows the HRSD-scores acquired at the same time points are given. Six out of twelve patients responded to ECT. Those results can be seen in the last column of Table 7.

Table 7: The first three columns represent the gCBF values per patient and MRI session in ml/100g/min. The last four columns include the HRSD-score at three time points and the response to ECT.

	Baseline	End-ECT	Follow-up	$HRSD_{base}$	$HRSD_{end}$	$HRSD_{fol}$	Response
sub-001	40.45	26.10	–	23	15	–	Non-responder
sub-003	30.70	38.34	35.74	17	4	2	Responder
sub-004	63.30	46.68	59.59	34	34	27	Non-responder
sub-006	41.29	37.4	28.85	18	13	23	Non-responder
sub-007	38.83	30.38	35.26	35	19	18	Non-responder
sub-008	62.38	40.84	34.88	27	24	31	Non-responder
sub-009	45.27	–	51.83	20	9	2	Responder
sub-011	18.63	25.57	–	26	11	–	Responder
sub-012	48.30	36.28	33.97	29	13	9	Responder
sub-013	46.02	43.40	52.97	32	12	23	Responder
sub-018	52.55	53.35	–	17	18	–	Non-responder
sub-020	22.68	24.33	–	19	7	–	Responder

$HRSD_{base}$= baseline Hamilton Rating Scale for Depression; $HRSD_{end}$ = HRSD within two weeks after last ECT session; $HRSD_{fol}$ = HRSD after three months.

3.3.1 Global CBF analysis

In the left panel of Figure 9, the HRSD-scores per patient are plotted against the moment of measurement. Ten out of twelve patients show a decrease in HRSD-score at end-ECT compared to baseline. Four out of eight patients show a continuing decrease in HRSD-score at follow-up. After an initial decrease at end-ECT the HRSD-score increased at follow-up in three patients. In one patient a small increase was seen at end-ECT followed by a decrease at follow-up. In the right panel of Figure 9, a decrease in HRSD-score is seen over time. Not only between baseline and end-ECT but also between end-ECT and follow-up. Hereby, it should be noticed that the data set at follow-up is not complete and consists of eight measurements. Over time the responders show an increase in gCBF whereas the non-responders show a decrease as can be seen in Figure 10. The baseline gCBF values of responders are lower compared to the non-responders.
The results of the first linear mixed-effects model testing the effect of normalised gCBF on normalised HRSD-score can be found in Table 8. The estimate of the dependent variable (normalised HRSD-score) was 1.282 ($SE = 0.330$) after correction for the effects age and sex. The normalised gCBF had a significant effect on the normalised HRSD-score ($p = 0.02$). Based on visual assessment of the Q-Q-plot, the residuals were not perfectly normally distributed.

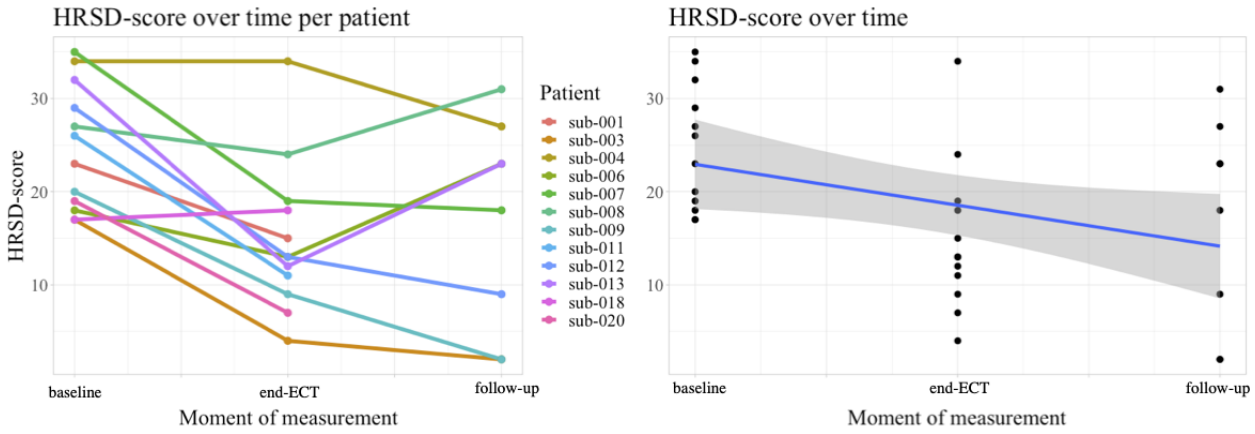

Figure 9: Left panel: HRSD-scores per patient at baseline, end-ECT and follow-up. Right panel: linear data fit of the data visualised in the left panel. The grey area indicates the 95% CI.

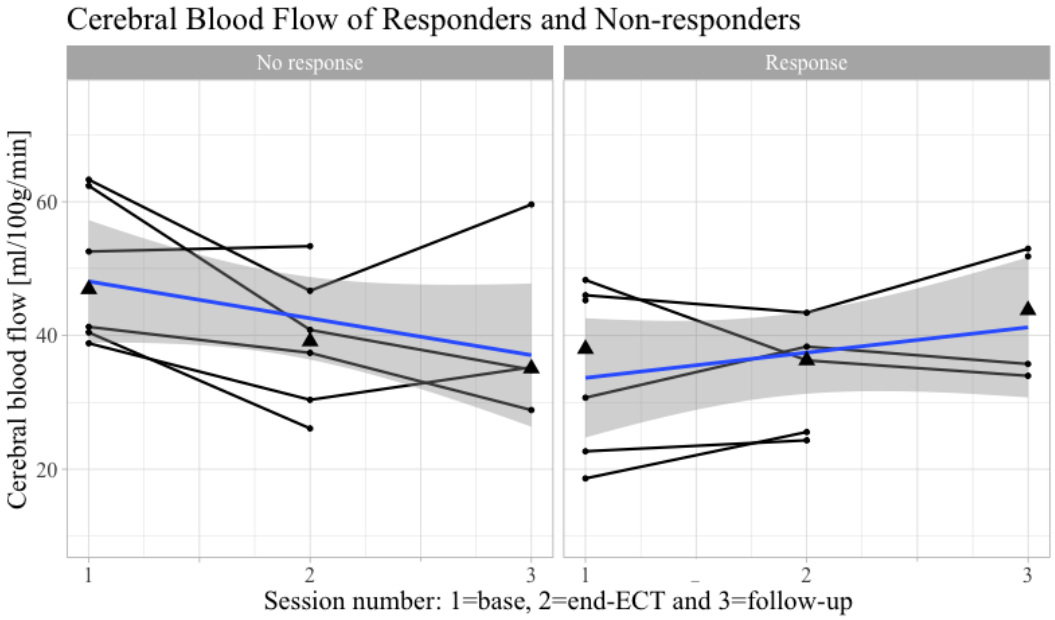

Figure 10: Patients were divided in non-responders (left panel) and responders (right panel) based on the HRSD-score. The course of gCBF values is visualised per patient and the black triangles represent the median at every time-point. In both figures a linear fit of the data is visualised in blue with the 95% CI depicted in grey.

Table 8: Results of linear mixed-effects model with normalised gCBF as fixed effect.

	Estimate	*SE*	df	*t*	*p*
End-ECT and follow-up					
Intercept normalised HRSD-score	1.282	0.330	10.113	3.886	2.974e-3 ***
Age	0.007	0.007	9.621	1.059	0.316
Sex male	-0.314	0.144	8.810	-2.172	0.059 .
Global CBF	-0.935	0.345	11.433	-2.708	0.020 *

SE= standard error, df = degrees of freedom, significance codes: 0 '***' 0.01 '*' 0.05 '.'

3.3.2 Regional CBF analysis

The normalised rCBF values for responders and non-responders in the six included regions can be seen in Figure 11. Compared to baseline all responders have a higher rCBF in all six regions in comparison with non-responders. The responders show an increase in rCBF at end-ECT compared to baseline in the amygdala, frontal lobe and hippocampus, as can be seen in Figure 11(a). At follow-up the responders show an increase in rCBF compared to baseline in five regions except for the parahippocampal cortex, see Figure 11(b). The non-responders show a decrease in rCBF in all regions at both end-ECT and follow-up compared to baseline.

The course of the rCBF per region over time, divided by responders and non-responders is visualised in Figure 12. In all regions, the responders have a lower rCBF start-value compared to non-responders. Except for the parahippocampal cortex, an increase in rCBF is seen in the responders and a decrease in the non-responders over time. The course of the rCBF in the amygdala and parahippocampal cortex was not as hypothesised. In the parahippocampal cortex, the rCBF values of both responders and non-responders decreased over time whereby the differences between both groups reduced. Variation is seen between the absolute rCBF values in the six regions.

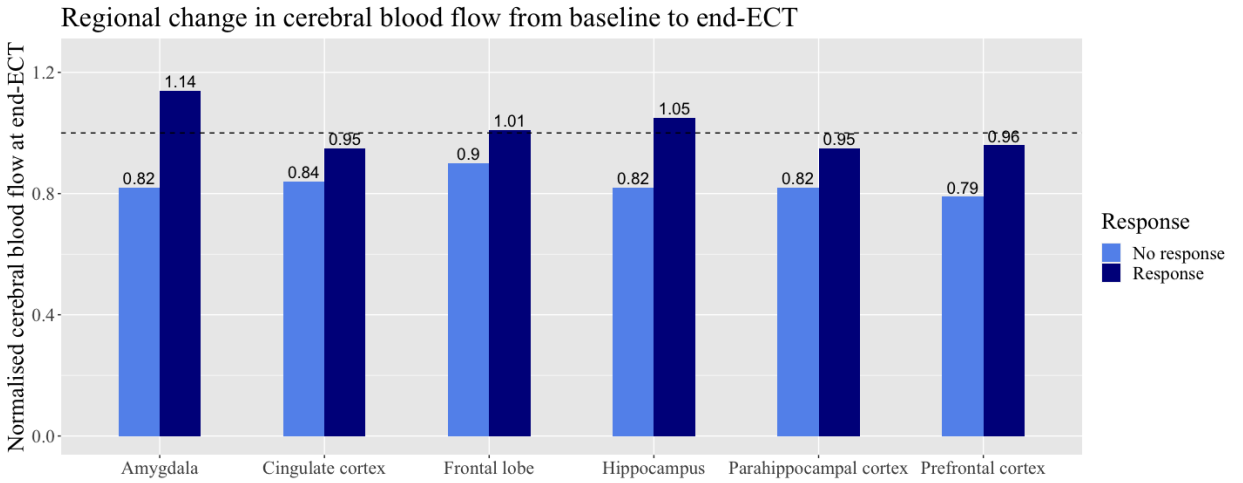

(a)

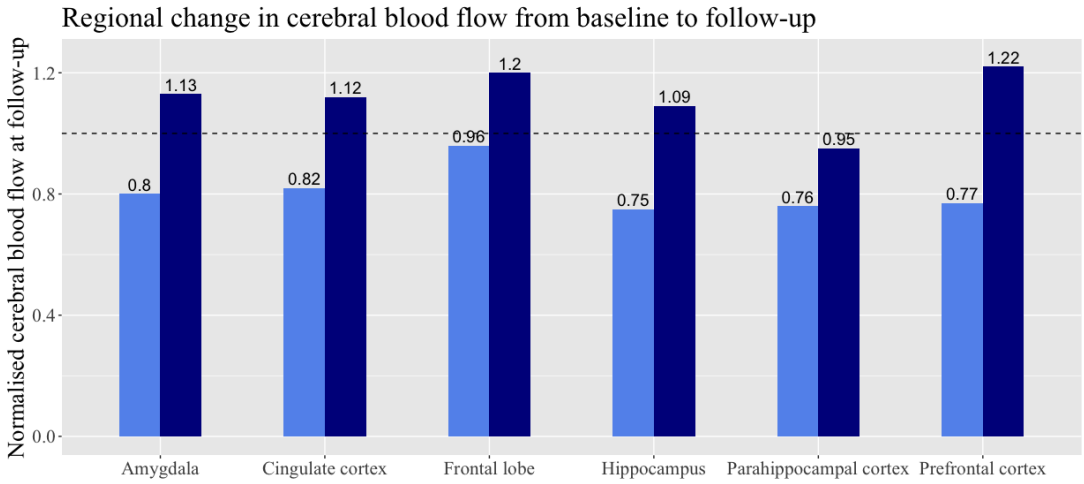

(b)

Figure 11: Regional CBF values in all included regions split in responders and non-responders. Normalised by dividing absolute values by corresponding baseline values. The dotted line at y=1 represents the transition between an increase or decrease in CBF a) Normalised CBF values at end-ECT, b) normalised CBF values at follow-up.

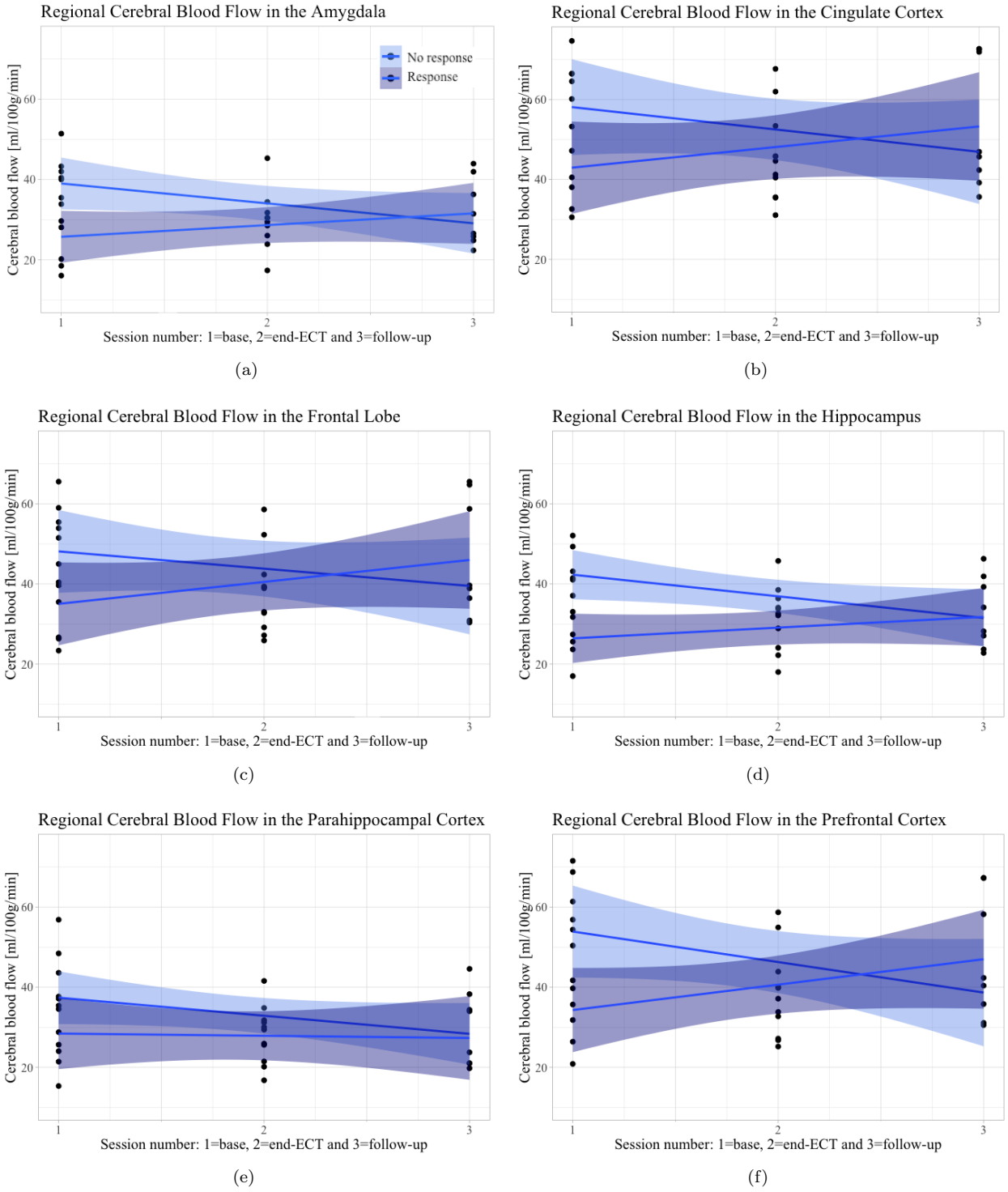

Figure 12: The course of absolute regional CBF values. Linear lines are with 95% CI, are included to fit the data of responders (dark-blue) and non-responders (light-blue) separately. a) amygdala, b) cingulate cortex, c) frontal lobe, d) hippocampus, e) parahippocampal cortex and f) prefrontal cortex.

The results of the second linear mixed-effects model, are listed in Table 9. No significant correlation was found between the normalised HRSD-score and age, sex or normalised rCBF in the six included regions. Based on visual assessment of the Q-Q-plot, the residuals were not perfectly normally distributed.

Table 9: Results of linear mixed-effects model with normalised rCBF of six regions as fixed effects.

	Estimate	*SE*	df	*t*	*p*
End-ECT and follow-up					
Intercept normalised HRSD-score	1.055	0.552	10	1.912	0.085
Age	0.002	0.011	10	0.170	0.868
Sex male	-0.233	0.146	10	-1.595	0.142
Amygdala	-1.105	0.930	10	-1.189	0.262
Cingulate cortex	1.759	1.245	10	1.413	0.188
Frontal lobe	0.189	0.712	10	0.265	0.796
Hippocampus	-0.521	1.334	10	-0.391	0.704
Prefrontal cortex	-1.195	0.992	10	-1.204	0.256
Parahippocampal cortex	0.496	0.789	10	0.629	0.544

SE= standard error, df = degrees of freedom

3.4 Discussion

We aimed to find the antidepressant effects of ECT in the brain. Neural function, in regions known to be affected in MDD, was assessed by rCBF measured based on pCASL MRI scans and combined with the clinical response by means of the HRSD-score. Half of the included patients responded to treatment and a decrease in HRSD-score was seen over the ECT course. The change in gCBF over the ECT course had a statistically significant effect on the change in HRSD-score in the same time frame. Responders had a lower mean baseline gCBF and rCBF in comparison with non-responders. A decrease in gCBF and rCBF in the amygdala, cingulate cortex, frontal lobe, hippocampus and prefrontal cortex was seen over the course of ECT in responders. The exact opposite was seen in non-responders for both gCBF and rCBF.

Change in gCBF and HRSD-score over the ECT course
Although on the lower side, the response rate in this study was comparable with values found in previous studies [1–3]. A significant correlation was found between the change in gCBF and in HRSD-score.
Bonne et al. defined a clinical response as a change in HRSD-score of at least 60% [41]. They found a significant global increase in CBF in patients that responded to ECT in accordance with the current study. These findings imply that reduced gCBF plays a role in MDD and can be reversed by effective treatment.

Course of CBF in responders and non-responders
Our results are in line with Leaver et al. [10], who found a lower pretreatment gCBF in responders compared to non-responders based on ASL MRI in a study with 57 included depressive patients. Accordingly, Awata et al. [42] found a significantly lower mean rCBF in ECT patients before treatment compared to controls. In their study, all patients responded to ECT and thus non-responders were not assessed. They utilised an ROI-based semiquantitative SPECT analysis with cerebellar normalisation, whereby eighty-five circular ROIs are combined into ten anatomical regions. However Järnum et al. [27] reported a significant decrease in rCBF in non-responders compared to healthy controls at baseline. Nevertheless, their definition for clinical response differed compared to the current study and previously mentioned studies. Only patients with an HRSD-score below seven were considered as responders which makes their results less comparable.
After ECT (both end-ECT and follow-up) a decrease in normalised rCBF in non-responders was found in all included regions in this study. Vangu et al. [43] also found unchanged or diminished rCBF in non-responders in the temporal regions, frontal regions, and anterior cingulate gyrus compared to baseline. Also, the increase in rCBF in responders found in this study was previously replicated [10, 41–43]. In the ROI-based analysis of Awata et al. [42] the mean rCBF of responders both at two weeks and three months after ECT increased significantly compared to baseline, thereby reaching the mean rCBF level of healthy controls. A comparable analysis was performed by Bonne et al. [41] who found a relative rCBF increase in responders five to eight days after ECT in the anterior and posterior cingulate, frontal and parietal cortices. Lastly, a study utilising pCASL just like in the current study, also found transiently increased gCBF in responders after two initial ECT sessions [10]. Our results and those of previous studies suggest that ECT responders have a lower gCBF and rCBF in specific regions at baseline that raises back to normal values after successful ECT. However, the mechanisms behind this potential link between lower baseline CBF and thus lower brain activity,

and antidepressant response are unknown. Reduced brain function before treatment could prevent neuronal hyperexcitability during treatment which can be harmful to neuronal cells. Also, neurons might have more capacity to respond to ECT induced seizure activity when baseline CBF values are lower. To further investigate this putative link, animal studies could be conducted on a cellular level. Clinical studies might explore whether an induced state of low CBF before ECT induced seizures improves the antidepressant response [10].

Change in rCBF and HRSD-score over the ECT course
A correlation between normalised rCBF and HRSD-score was seen in five out of six regions. Hereby, the influence of the HRSD-score was included by dividing the patients into responders and non-responders. However, no statistically significant correlations were found. In the previously described study by Bonne et al. [41] a significant change in rCBF in the anterior and posterior cingulate gyrus, and in the frontal and parietal regions was reported in patients that responded to ECT whereas no changes were found in non-responders. Accordingly, Milo et al. [44] concluded that statistically significant rCBF changes, specifically in the frontal and parietal regions in the brain, only occurred in patients with an excellent clinical response to ECT. They utilised 99mTc-SPECT and assessed the rCBF two to three days before the first ECT session and four days after termination of the treatment. On the other hand, Segawa et al. [12] did not find positive correlations between rCBF changes and HRSD-changes. Nevertheless, they reported a strong significant negative correlation between the rCBF in the left amygdala and the HRSD-score, as was hypothesised based on literature [23, 31–33] but not found in the current study. Also, Segawa et al. made 99mTc-SPECT images before the first ECT session and within three to twenty days after the last ECT session. Based on the results of the current study and previous literature, a correlation between changes in rCBF and HRSD-score over the ECT course is suggested.

Limitations
The small study population made the results less representative. Including an adequate number of patients based on a power calculation could generate more reliable conclusions. But *a priori* power calculation was aggravated by the novelty of this line of research. Moreover, pairing included subjects with matching healthy controls may give more information about the variability of CBF over time which could be corrected for within the analyses. Another disadvantage was the limited number of regions included in the current study. Based on literature, six regions that are suggested to have diminished rCBF in MDD patients were included. Nevertheless, like other abnormalities of higher mental functions, the precise locations and manifestations of depression in the brain are difficult to assess and may differ per individual [19]. Thus, important regions could be missed in the current analysis. Utilising a generalised linear model based on global imaging data could give more information about the regions involved. This study may be prone to selection bias because only cooperative depressed patients could be included. Lastly, the residuals of both mixed-effects models were not perfectly normally distributed. Therefore, results are susceptible to overinterpretation.

Clinical relevance
ECT responders seem to have a decreased gCBF and rCBF that can return to normal values after successful ECT. This suggests that reduced CBF could be a state marker for MDD rather than a trait abnormality. However, it has become increasingly difficult to interpret all the reported changes in local perfusion in MDD related to get one widely applicable standard for this state marker. The baseline difference in rCBF between responders and non-responders may also imply a dichotomy in MDD-patients. It is speculated that MDD might lead to impaired CBF in one group and affects the brain in other ways in the second group. Patients in the first group may benefit from ECT whereas the patients in the second group do not because it does not treat their cause of depression. This theory might explain why certain patients do benefit from ECT and others do not.

Conclusion
ECT responders and non-responders differed in global and regional CBF values at baseline and across the ECT course. This suggests that pCASL MRI based CBF might be utilised as an objective marker for treatment response in MDD. Nevertheless, MDD is a complex and heterogeneous disease that can not only be explained by perfusion changes. Conducting a voxel-based regional analysis on the complete data set of SYNAPSE may give more information in the future.

References

[1] L. van Diermen, S. van den Ameele, A. M. Kamperman, B. C. G. Sabbe, T. Vermeulen, and D. Schrijvers. Prediction of electroconvulsive therapy response and remission in major depression: meta-analysis. *The British Journal of Psychiatry*, 212:71–80, 2018.

[2] A. U. Haq, A. F. Sitzmann, M. L. Goldman, D. F. Maixner, and B. J. Mickey. Response of depression to electroconvulsive therapy: a meta-analysis of clinical predictors. *The Journal of clinical psychiatry*, 76:1374–1384, 2015.

[3] B. Dierckx, W.T. Heijnen, W.W. van den Broek, and T.K. Birkenhäger. Efficacy of electroconvulsive therapy in bipolar versus unipolar major depression: a meta-analysis. *Bipolar Disorders*, 14:146–150, 3 2012. https://doi.org/10.1111/j.1399-5618.2012.00997.x.

[4] W. W. van den Broek, T. K. Birkenhäger, D. de Boer, J. P. Burggraaf, B. van Gemert, and T. H.N. Groenland. *Richtlijn Elektroconvulsietherapie*. De Tijdstroom, second edi edition, 2010.

[5] J. A. Van Waarde and M. J. A. M. Van Putten. Anatomie en neurofysiologie, 2019.

[6] H. Blumenfeld, M. Westerveld, R. B. Ostroff, S. D. Vanderhill, J. Freeman, and A. Necochea. Selective frontal, parietal, and temporal networks in generalized seizures. *NeuroImage*, 19:1556–1566, 8 2003.

[7] M. Enev, K. A. McNally, G. Varghese, I. G. Zubal, R. B. Ostroff, and H. Blumenfeld. Imaging onset and propagation of ect-induced seizures. *Epilepsia*, 48, 2 2007.

[8] H. Takano, N. Motohashi, T. Uema, K. Ogawa, T. Ohnishi, and M. Nishikawa. Changes in regional cerebral blood flow during acute electroconvulsive therapy in patients with depression: positron emission tomographic study. *The British journal of psychiatry : the journal of mental science*, 190:63–68, 1 2007.

[9] T. Suwa, C. Namiki, S. Takaya, A. Oshita, K. Ishizu, and H. Fukuyama. Corticolimbic balance shift of regional glucose metabolism in depressed patients treated with ect. *Journal of Affective Disorders*, 136:1039–1046, 2012.

[10] A.M. Leaver, M. Vasavada, S.H. Joshi, B. Wade, R.P. Woods, and R. Espinoza. Mechanisms of antidepressant response to electroconvulsive therapy studied with perfusion magnetic resonance imaging. *Biological Psychiatry*, 85:466–476, 2019.

[11] H. Takano, M. Kato, A. Inagaki, K. Watanabe, and H. Kashima. Time course of cerebral blood flow changes following electroconvulsive therapy in depressive patients-measured at 3 time points using single photon emission computed tomography. *The Keio Journal of Medicine*, 55:153–160, 2006.

[12] K. Segawa, H. Azuma, K. Sato, T. Yasuda, K. Arahata, and K. Otsuki. Regional cerebral blood flow changes in depression after electroconvulsive therapy. *Psychiatry Research: Neuroimaging*, 147:135–143, 2006.

[13] A.M. Leaver, M. Vasavada, A. Kubicki, B. Wade, J. Loureiro, G. Hellemann, S.H. Joshi, R.P. Woods, R. Espinoza, and K.L. Narr. Hippocampal subregions and networks linked with antidepressant response to electroconvulsive therapy. *Molecular Psychiatry*, 2020.

[14] S. H. Joshi, R. T. Espinoza, T. Pirnia, J. Shi, Y. Wang, and A. Leaver. Structural plasticity of the hippocampus and amygdala induced by electroconvulsive therapy in major depression. *Biological Psychiatry*, 79:282–292, 2016.

[15] C. C. Abbott, N. T. Lemke, S. Gopal, R. J. Thoma, J. Bustillo, and V. D. Calhoun. Electroconvulsive therapy response in major depressive disorder: a pilot functional network connectivity resting state fmri investigation. *Frontiers in psychiatry*, 4:10, 2013.

[16] J. A. van Waarde, H. S. Scholte, L. J. B. van Oudheusden, B. Verwey, D. Denys, and G. A. van Wingen. A functional mri marker may predict the outcome of electroconvulsive therapy in severe and treatment-resistant depression. *Molecular Psychiatry*, 20:609–614, 2015.

[17] M. S. Nobler, H.A. Sackeim, I. Prohovnik, J. R. Moeller, S. Mukherjee, and D.B. Schnur. Regional cerebral blood flow in mood disorders, iii. treatment and clinical response. *Archives of general psychiatry*, 51:884–897, 11 1994.

[18] I. Tendolkar, M. van Beek, I. van Oostrom, M. Mulder, J. Janzing, and R. Oude Voshaar. Electroconvulsive therapy increases hippocampal and amygdala volume in therapy refractory depression: A longitudinal pilot study. *Psychiatry Research: Neuroimaging*, 214:197–203, 2013.

[19] M. Pandya, M. Altinay, D. A. Malone Jr, and A. Anand. Where in the brain is depression? *Current psychiatry reports*, 14:634–642, 12 2012.

[20] M. Ota, T. Noda, N. Sato, K. Hattori, T. Teraishi, and H. Hori. Characteristic distributions of regional cerebral blood flow changes in major depressive disorder patients: a pseudo-continuous arterial spin labeling (pcasl) study. *Journal of affective disorders*, 165:59–63, 8 2014.

[21] T. C. Ho, J. Wu, D. D. Shin, T. T. Liu, S. F. Tapert, and G. Yang. Altered cerebral perfusion in executive, affective, and motor networks during adolescent depression. *Journal of the American Academy of Child Adolescent Psychiatry*, 52:1076–1091.e2, 2013.

[22] S. Lui, L. M. Parkes, X. Huang, K. Zou, R. C. K. Chan, and H. Yang. Depressive disorders: Focally altered cerebral perfusion measured with arterial spin-labeling mr imaging. *Radiology*, 251:476–484, 5 2009. doi: 10.1148/radiol.2512081548.

[23] W. C. Drevets, J. L. Price, J. R. Simpson, R. D. Todd, T. Reich, and M. Vannier. Subgenual prefrontal cortex abnormalities in mood disorders. *Nature*, 386:824–827, 1997.

[24] M. Liotti and H. S. Mayberg. The role of functional neuroimaging in the neuropsychology of depression. *Journal of Clinical and Experimental Neuropsychology*, 23, 2 2001.

[25] S. Rigucci, G. Serafini, M. Pompili, G. D. Kotzalidis, and R. Tatarelli. Anatomical and functional correlates in major depressive disorder: The contribution of neuroimaging studies. *The World Journal of Biological Psychiatry*, 11:165–180, 3 2010. doi: 10.3109/15622970903131571.

[26] N. Vasic, N. D. Wolf, G. Grön, Z. Sosic-Vasic, B. J. Connemann, and F. Sambataro. Baseline brain perfusion and brain structure in patients with major depression: a multimodal magnetic resonance imaging study. *Journal of psychiatry neuroscience : JPN*, 40:412–421, 11 2015.

[27] H. Järnum, S. F. Eskildsen, E. G. Steffensen, S. Lundbye-Christensen, C. W. Simonsen, and I. S. Thomsen. Longitudinal mri study of cortical thickness, perfusion, and metabolite levels in major depressive disorder. *Acta Psychiatrica Scandinavica*, 124:435–446, 12 2011. https://doi.org/10.1111/j.1600-0447.2011.01766.x.

[28] C. A. M. Périco, C. R. Skaf, A. Yamada, F. Duran, C. A. Buchpiguel, and C. C. Castro. Relationship between regional cerebral blood flow and separate symptom clusters of major depression: A single photon emission computed tomography study using statistical parametric mapping. *Neuroscience Letters*, 384:265–270, 2005.

[29] A. Graff-Guerrero, J. González-Olvera, Y. Mendoza-Espinosa, V. Vaugier, and J. C. Garcıa-Reyna. Correlation between cerebral blood flow and items of the hamilton rating scale for depression in antidepressant-naive patients. *Journal of Affective Disorders*, 80:55–63, 2004.

[30] H. S. Mayberg. Frontal lobe dysfunction in secondary depression. *The Journal of Neuropsychiatry and Clinical Neurosciences*, 6, 11 1994.

[31] W. C. Drevets. Neuroimaging studies of mood disorders. *Biological Psychiatry*, 48:813–829, 2000.

[32] M. Hornig, P. David Mozley, and J. D. Amsterdam. Hmpao spect brain imaging in treatment-resistant depression. *Progress in Neuro-Psychopharmacology and Biological Psychiatry*, 21:1097–1114, 1997.
[33] G. J. Siegle, S. R. Steinhauer, M. E. Thase, V. A. Stenger, and C. S. Carter. Can't shake that feeling: event-related fmri assessment of sustained amygdala activity in response to emotional information in depressed individuals. *Biological Psychiatry*, 51:693–707, 2002.
[34] A. M. Leaver, R. Espinoza, T. Pirnia, S. H. Joshi, R. P. Woods, and K. L. Narr. Modulation of intrinsic brain activity by electroconvulsive therapy in major depression. *Biological Psychiatry: Cognitive Neuroscience and Neuroimaging*, 1:77–86, 2016.
[35] C. C. Abbott, T. Jones, N. T. Lemke, P. Gallegos, S. M. McClintock, and A. R. Mayer. Hippocampal structural and functional changes associated with electroconvulsive therapy response. *Translational psychiatry*, 4:e483, 11 2014.
[36] Y. I. Sheline, M. Sanghavi, M. A. Mintun, and M. H. Gado. Depression duration but not age predicts hippocampal volume loss in medically healthy women with recurrent major depression. *The Journal of Neuroscience*, 19:5034, 6 1999.
[37] P. Videbech, B. Ravnkilde, T. H. Pedersen, H. Hartvig, A. Egander, and K. Clemmensen. The danish pet/depression project: clinical symptoms and cerebral blood flow. a regions-of-interest analysis. *Acta Psychiatrica Scandinavica*, 106, 7 2002.
[38] C. Cusin, H. Yang, A. Yeung, and M. Fava. Rating scales for depression, 2010.
[39] M. HAMILTON. A rating scale for depression. *Journal of neurology, neurosurgery, and psychiatry*, 23:56–62, 2 1960.
[40] R Core Team. R: A language and environment for statistical computing., 2021.
[41] O. Bonne, Y. Krausz, B. Shapira, M. Bocher, H. Karger, and M. Gorfine. Increased cerebral blood flow in depressed patients responding to electroconvulsive therapy. *Journal of Nuclear Medicine*, 37:1075, 7 1996.
[42] S. Awata, M. Konno, R. Kawashima, K. Suzuki, T. Sato, and H. Matsuoka. Changes in regional cerebral blood flow abnormalities in late-life depression following response to electroconvulsive therapy. *Psychiatry and Clinical Neurosciences*, 56:31–40, 2 2002. https://doi.org/10.1046/j.1440-1819.2002.00927.x.
[43] M. D. T. Vangu, J. D. Esser, I. H. Boyd, and M. Berk. Effects of electroconvulsive therapy on regional cerebral blood flow measured by 99mtechnetium hmpao spect. *Progress in Neuro-Psychopharmacology and Biological Psychiatry*, 27:15–19, 2003.
[44] T. J. Milo, G. E. Kaufman, W. E. Barnes, L. M. Konopka, J. W. Crayton, and J. G. Ringelstein. Changes in regional cerebral blood flow after electroconvulsive therapy for depression. *The Journal of ECT*, 17, 2001.

Conclusions

This thesis was focused on assessing the short term (postictal) and long term (weeks to months after treatment) effects of ECT on CBF in depressed patients. Although we observed a decrease in postictal CBF compared to baseline in the majority of patients, the differences were not statistically significant. These findings do not support the hypothesis of postictal hypoperfusion. Limitations concern variation in the moment of CBF measurement, small sample size, and using mean postictal CBF maps which resulted in less reliable results. Longer seizure duration resulted in lower perfusion and therefore might also be related to more postictal symptoms. Future research should focus on exact timing of ASL acquisition and higher sample sizes. Moreover, the long term antidepressant effects of ECT on the CBF were assessed. The normalised gCBF seems to be related to overall perfusion. This effect could not be replicated for normalised rCBF. Moreover, responders had lower mean baseline CBF values and showed an increase over the course of the ECT. Whereas, non-responders showed a decrease. There seems to be a relation between CBF and antidepressant effect of ECT whereby responders and non-responders already show differences in CBF at baseline. This study highlights perfusion-based differences in ECT responders and non-responders, paving new paths for treatment options and future research.

Acknowledgements

I am grateful that I was able to go to university and made the right choice by moving across the country for my studies. After more than seven years this thesis marks the end of my time as a student. I enjoyed every phase and will always look back with gratitude.

I would like to express my appreciation to the members of my committee for their guidance and support during my gradation internship. Michel, although we did not meet often your ideas and different points of view were always very inspiring. Jeannette, you were always very approachable and your expertise and feedback encouraged me to develop. Moreover, you taught me to make a strong appearance without saying 'beetje' ;). Julia, I find your inexhaustible perseverance and enthusiasm admirable. You gave me the feeling that I was part of SYNAPSE and thought me a lot about all facets of your research. Paul, over the last two years you really got to know me on a professional and personal level. I very much appreciate your support in difficult times and while making difficult decisions. David, thank you for being the MRI supervisor I needed, for all the insightful brainstorm sessions on Tuesdays and for providing me with useful connections.

Other people also played an important role in my graduation. Jeroen, meetings with you always led to fresh ideas and new perspectives. Thank you for investing your time into reviewing my thesis. Joey, you were as a second process supervisor to me. You taught me a lot about myself and my ways of dealing with this large project. Sophie and Lena from the LUMC, your expertise on ASL MRI and FSL was exactly what I needed. Thank you very much for helping me out with my project. I also would like to thank all neuro-researchers at Rijnstate, Astrid, Hanneke, Marlous, Nicole and especially Sven, for great brainstorm sessions during the meetings and a fun working environment. Many thanks to Oscar, who plays a vital part in enabling research at the Psychiatry department. And to Marleen, whose voluntary work is essential to conduct all measurements within the SYNAPSE.

Special thanks to Robert, without your support, care, patience and love I would not stand, were I stand today. Thank you for always being there. Last but not least, I want to thank my parents and brother for their support and guidance during this graduation internship and its difficult times.

Eva Aalbregt

Arnhem, November 2021

Appendices

Appendix I: Registration of the T_1-weighted images and pre-made CBF maps

The self-made CBF maps were available in standard space. But the T_1-weighted images and pre-made CBF maps had to be registered to standard space to enable further processing and group analyses. An overview of the complete registration of both images is seen in Figure A1. The first step was linear registration of the T_1-weighted image to standard space. Brain extracted images served as input for FLIRT to ensure an optimal result. One of the output measures of FLIRT was a 4x4 affine matrix which included information about how to register the input (T_1-weighted image) to the reference (standard MNI152 brain). That affine matrix served as input for the non-linear registration of the T_1-weighted image to standard space. Also, the full T_1-weighted image and full MNI152 2mm image served as input, see Figure A1 B. Unlike FLIRT, FNIRT performs best with non-brain extracted input images. Predefined configuration files containing all parameters needed for specific registrations are available within FNIRT. The configuration file for registration from structural space to standard space was the last input for FNIRT. The result of FNIRT consisted of a warp-field and T_1-weighted image in standard space. A warp is the parametric model that explains the deformation between the input image and the image to register to.
Registration of the pre-made CBF map could not be executed in the same way as the T_1-weighted image. A configuration file for the non-linear registration from a CBF map to standard space was not available. And generating personal configuration files was discouraged by the developers of FNIRT. A different approach was executed whereby the configuration file for registration from structural to standard space, was utilised see Figure A1 C and D. The process was started with linear registration of the pre-made CBF map to structural space. The resulting affine transformation matrix served as input for APPLYWARP. The warp is derived from the non-linear registration of the T_1-weighted image to standard space, see Figure A1 B. Thus, APPLYWARP received information both on how to register the CBF map to structural space and on how to non-linearly register structural space to standard space. By combining these inputs with the reference image (MNI152) and the brain extracted pre-made CBF map a non-linear registration to standard space was achieved with APPLYWARP.

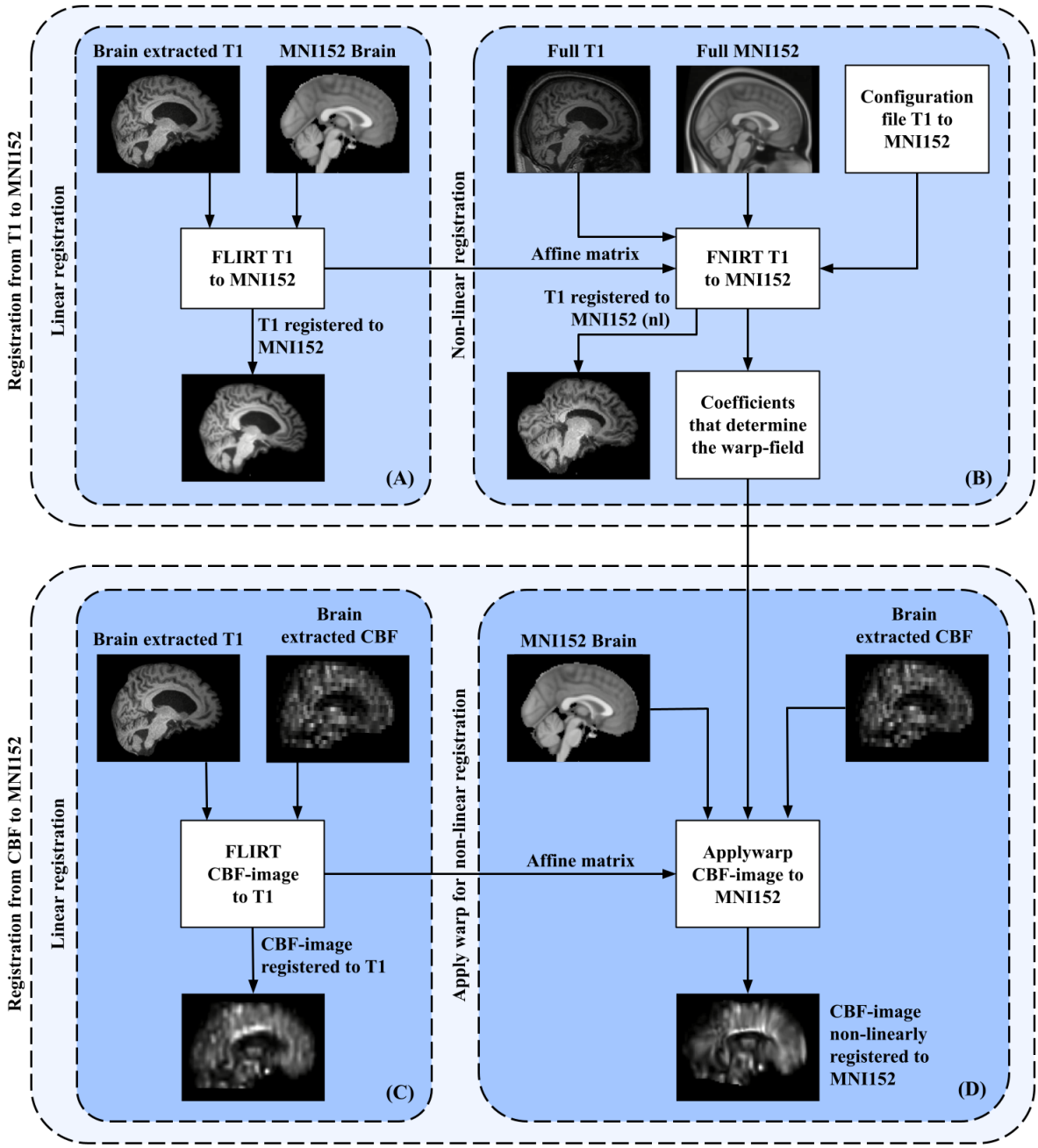

Figure A1: For the non-linear registration of the pre-made CBF map to standard space, four operations, part of two distinct registrations were needed. A) Linear registration from the T_1-weighted image to standard space, resulting in a 4-by-4 affine transformation matrix. B) Non-linear registration from the T_1-weighted image whereby the transformation matrix generated in A) served as input in addition to the full T_1-weighted image, full MNI152 image and configuration file, resulting in a 4D NIfTI-file containing the spline coefficients which were used in D). C) Linear registration of pre-made CBF map to structural space. D) Combining all pre-processing steps by using APPLYWARP.